Characterization of unique subregions of the caudal lateral striatum:

In their conserved expression patterns of dopamine receptors D1 and D2 in rodents and primates

DOCTORAL DISSERTATION

A thesis submitted in partial fulfillment
of the requirements for the degree of
Doctor of Philosophy

By:
Kumiko Ogata

Supervisor:
Dr. Yoshio Sakurai

Graduate School of Brain Science
Doshisha University
March 2021
Kyoto, Japan

Abstract

In the present study, we conducted a detailed morphological investigation of distinct caudal lateral striatum subregions with the unique expression pattern for dopamine receptor D1 (D1R) and D2 (D2R). It was generally accepted that D1R- and D2R-expressing neurons are homogeneously and randomly distributed throughout the striatum. However, previous studies reported novel striatal subregions exhibiting distinct expression patterns of dopamine receptors, using reporter transgenic mice expressing marker proteins under either D1R or D2R promoter. They demonstrated the presence of the D1R-poor zone, in which D2R-expressing neurons are predominant, and the D2R-poor zone, in which D1R-expressing neurons are predominant. These D1R- and D2R-poor zones were next to each other in the caudal lateral striatum adjacent to the globus pallidus (GP). The present study aimed to characterize the distribution of endogenous dopamine receptors and the cell composition of the D1R- and D2R-poor zones in non-transgenic animals, and demonstrated where these distinct subregions project to. We found that 1) the D1R-poor zone comprises only 12% of D1R mRNA-positive neurons and 79% of D2R mRNA-positive neurons, whereas the D2R-poor zone comprises 82% of D1R mRNA-positive neurons and only 4% of D2R mRNA-positive neurons, 2) dopaminergic axons were sparse, whereas serotonergic axons were more abundant in the D1R- and D2R-poor zones, 3) the general relationships of D1R-direct pathway medium spiny neurons (dMSNs) and D2R-indirect pathway medium spiny neurons (iMSNs) were conserved in these distinct subregions, 4) D1R- and D2R-poor zones are conserved not only in mice and rats but also in marmosets, 5) MSNs in the D1R- and D2R-poor zones preferentially project to the GP and the substantia nigra pars lateralis (SNL), but not the entopeduncular nucleus, and 6) dMSNs in the D1R- and D2R-poor zones preferentially project to the dorsal part of the SNL and especially project to the parvalbumin-positive GABAergic neurons in the SNL. These results suggest that the D1R- and D2R-poor zones are conserved not only in rodents but also in primates, and form neural circuits that differ from those in other striatal areas. Furthermore, the D1R- and D2R-poor zones are thought to be located in the tail of the striatum, which is known to be a distinct subregion with neural circuits and functions that differ from those of other striatal areas. The present study elucidated the anatomical characterization of the D1R- and D2R-poor zones and might represent a key step toward understanding the basal ganglia circuit and function.

Acknowledgement

First, I would like to express my sincere gratitude to my advisor, Prof. Yoshio Sakurai, for his support, invaluable guidance and teachings, and all the aid I received regarding this research and the writing of this thesis.

I also extend my feelings of gratitude to members of my thesis reviewing committee—Prof. Nobuyuki Nukina, Prof. Hiroaki Misono, and Prof. Susumu Takahashi—for their encouragement, insightful comments, and meaningful questions.

I would also like to thank to Prof. Kenta Kobayashi for providing the specific virus vectors, Dr. Kenichi Inoue for providing common marmoset brains, and Mr. Shinichiro Okamoto for providing in situ hybridization probes for Drd1 and Drd2 required for my research.

Furthermore, I thank my ex-lab members from the neural circuitry group—Prof. Fumino Fujiyama, Dr. Fuyuki Karube, Dr. Yasuharu Hirai, Dr. Yoon-Mi Oh, Dr. Kazuko Mizutani, Dr. Yasutake Nakano, Mr. Tetsuya Higashiyama, and Ms. Fuko Kadono—for their time, support, and helpful comments.

Last but not the least, I would like to thank my family for supporting me spiritually throughout my life.

Table of contents

Table of Figures

Abbreviation list

Str: striatum

DS: dorsal striatum

GP: globus pallidus

EP: entopeduncular nucleus

STN: subthalamic nucleus

SN: substantia nigra

SNc: substantia nigra pars compacta

SNr: substantia nigra pars reticulata

SNL: substantia nigra pars lateralis

ASt: amygdalo-striatal transition area

ic: internal capsule

Cx: cortex

TEa: temporal association cortex

AUDp: primary auditory cortex

IC: inferior colliculus

MGm: medial division of the medial geniculate body

rDS: rostral part of the dorsal striatum

cDS: caudal part of the dorsal striatum

dSNL: dorsal part of the SNL

vSNL: ventral part of the SNL

dlSNr: dorsolateral part of the SNr

vlSNr: ventrolateral part of the SNr

dMSNs: direct pathway medium spiny neurons

iMSNs: indirect pathway medium spiny neurons

D1R: dopamine receptor D1

D2R: dopamine receptor D2

D2R-poor zone: D2R-expressing MSNs-poor zone

CDh: head of the caudate nucleus

CDt: tail of the caudate nucleus

TS: tail of the striatum

DAT: dopamine transporter

Enk: enkephalin

GABA: gamma-aminobutyric acid

PPE: preproenkephalin

SP: substance P

PV: parvalbumin

TH: tyrosine hydroxylase

AAV: adeno-associated virus vector

CTB: cholera-toxin subunit B

CTB555: CTB – Alexa Fluor 555 conjugate

CTB488: CTB – Alexa Fluor 488 conjugate

BDA: biotinylated dextran amine

PHA-L: Phaseolus vulgaris leucoagglutinin

LM: lateromedial

AP: anteroposterior

PB: phosphate buffer

PBS: phosphate-buffered saline

RT: room temperature

AIB: antibody incubation buffer

TBS: Tris-buffered saline

PFA: paraformaldehyde

0.1 M PB-DEPC: 0.1 M PB containing 0.1% diethylpyrocarbonate

DIG: digoxigenin

FITC: fluorescein isothiocyanate

NLS: N-lauroylsarcosine

RNase A: ribonuclease A

TNT: TS7.5 containing 0.05% Tween-20

PBST: Triton X-100

SSC: saline sodium citrate

ABC: avidin-biotin-peroxidase complex

NBT: 5-bromo-4-chloro-3-indolyl-phosphate

BCIP: nitro blue tetrazolium

DAB: diaminobenzidine-4HCl

MFM: epifluorescence microscope

ANOVA: analysis of variance

Chapter 1. General introduction

1. 1. The basal ganglia network model

The basal ganglia are involved in motor control, reward-based learning, and emotion, and are composed of multiple nuclei: the striatum, the globus pallidus (GP), the entopeduncular nucleus (EP), the subthalamic nucleus (STN), and the substantia nigra (SN). The striatum is an input nucleus of the basal ganglia and receives excitatory inputs from the cortex and the thalamus (Fig. 1). Approximately 77–95% of striatal neurons are projection neurons, and rest are interneurons (Gerfen and Surmeier, 2011). There are two types of projection neurons, direct pathway medium spiny neurons (dMSNs) and indirect pathway medium spiny neurons (iMSNs), which are clearly segregated in terms of both molecular expression and projections. dMSNs express gamma-aminobutyric acid (GABA), dynorphin, substance P (SP), and dopamine receptor D1 (D1R) and directly send inhibitory projections to the output nuclei of the basal ganglia, that is, the SN and the EP (Alexander and Crutcher, 1990; Gerfen and Surmeier, 2011). These output nuclei autonomously inhibit the thalamus and other brain areas. The release of this autonomous inhibition, namely disinhibition, is in response to inhibitory inputs from the dMSNs, which are activated by excitatory inputs from the cortex and the thalamus. As a result, the direct pathway plays a facilitating role (Nambu et al., 2002). iMSNs express GABA, preproenkephalin (PPE), and dopamine receptor D2 (D2R) and indirectly send inhibitory projections to the output nuclei via the GP and the STN (Alexandar and Crutcher, 1990; Gerfen and Surmeier, 2011). The output nuclei are released from autonomous inhibition by inhibitory

inputs from the GP, which receives inhibitory projections from iMSNs. Therefore, the output nuclei inhibit the thalamus and other brain areas. As a result, the indirect pathway plays a suppression role. The different circuitries and opposing functions of the direct and indirect pathways have been reported in morphological and electrophysiological studies on primates and rodents (DeLong et al., 1985; Robledo and Ferger, 1990; Kincaid et al., 1991; Kita and Kitai, 1991; Wichmann et al., 1994; Jaeger et al., 1995; Parent and Hazrati, 1995a; Parent and Hazrati, 1995b; Bergman et al., 1998; Mounir and Parent, 2002). Dopaminergic neurons from the substantia nigra pars compacta (SNc) play an important modulatory function as modulators regulating dMSNs and iMSNs through their axons which are spread widely in the striatum (Matsuda et al., 2009). dMSNs are activated through D1Rs, while iMSNs are modified to suppress through D2Rs.

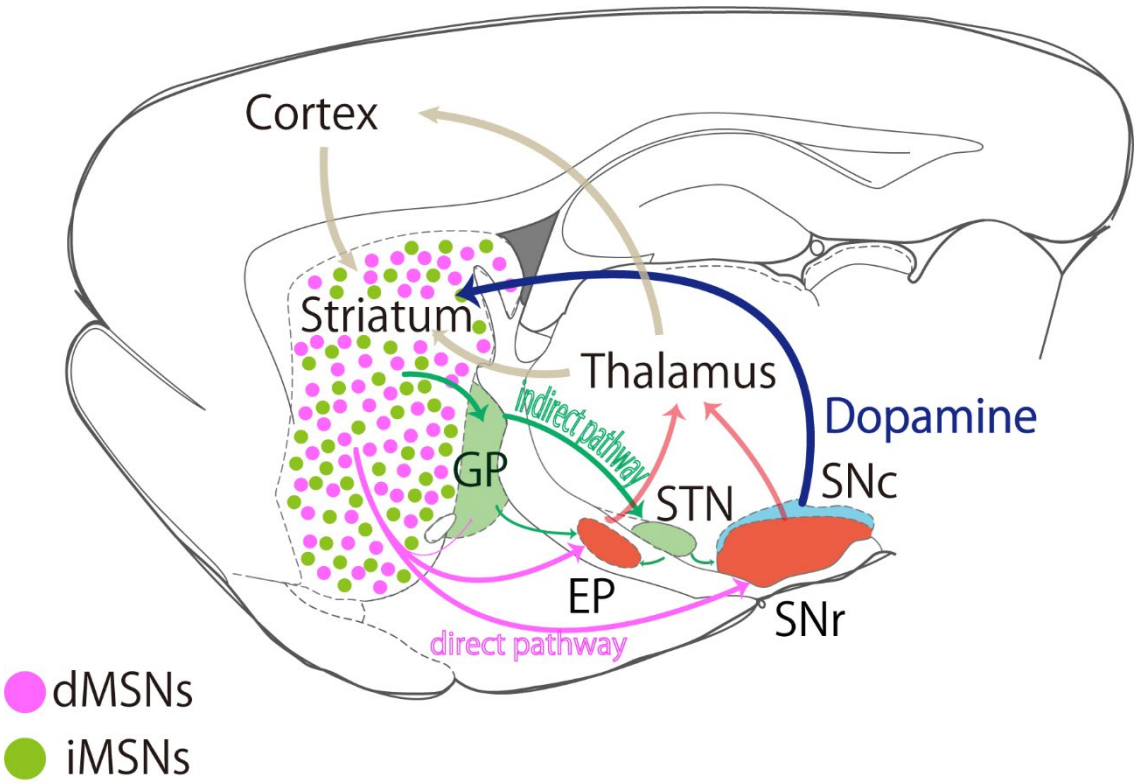

Fig. 1 Schematic representation of the basal ganglia network model

The striatum receives excitatory inputs from the cortex and the thalamus. Striatal information is sent to the output nuclei through two pathways. One is the direct pathway (pink arrows): direct pathway medium spiny neurons (dMSNs) directly project to the output nuclei—the entopeduncular nucleus (EP) and the substantia nigra pars reticulata (SNr). The other is the indirect pathway (green arrows): indirect pathway medium spiny neurons (iMSNs) send striatal information to the output nuclei via the globus pallidus (GP) and the subthalamic nucleus (STN). These two pathways are modified by the inputs of dopaminergic neurons from the substantia nigra pars compacta (SNc) (dark blue arrow).

1. 2. Distribution of striatal projection neurons in the mouse caudal lateral striatum

The striatum has striosome/matrix compartmentalization but lacks a well-organized cytoarchitecture, unlike the layered cortex and hippocampus. Therefore, dMSNs, iMSNs, and striatal interneurons were thought to be homogeneously and randomly distributed throughout the striatum (Lanca et al., 1986; Gerfen, 1989). However, Gangarossa and colleagues recently used Drd2-EGFP and Drd1a-EGFP hemizygous mice to report a subregion of the caudal lateral striatum that contains mostly MSNs expressing D1R but lacks D2R-expressing MSNs, and named it the D2R-expressing MSNs-poor zone (D2R-poor zone) (Gangarossa et al., 2013). This D2R-poor zone is located in the mouse caudal lateral striatum adjacent to the GP. Furthermore, Miyamoto and colleagues used transgenic mice expressing D1R-DARPP-32-Flag/D2R-DARPP-32-Flag-Myc and reported another striatal subregion, lacking MSNs expressing D1R, located adjacent to the D2R-poor zone in the caudal lateral striatum (Miyamoto et al., 2019). These findings suggest that the striatum does contain organized cytoarchitectures that form unique neuronal pathways for specific functions. However, it is essential to identify the distribution of endogenous dopamine receptors in the caudal lateral striatum and confirm the presence of the D1R-poor zone and the D2R-poor zone, because the expression of the marker proteins in the transgenic animals may become leaky or erroneous and may not faithfully reflect the expression patterns of endogenous receptors.

1. 3. The tail of the striatum in rodents

It is notable that the D1R- and D2R-poor zones are thought to be located in the tail of the striatum

(TS), which is reported by Menegas and colleagues (Menegas et al., 2015) in the first report on the functional differences between the TS and other striatal areas in rodents. Dopaminergic neurons are known to respond to the reward prediction error, the difference between actual and expected reward values, in rodents and primates (Bayer and Glimcher, 2005; Bromberg-Martin et al., 2010; Clark et al., 2012; Cohen et al., 2012; Schultz et al., 1997; Schultz, 1998; Schultz, 2007; Eshel et al., 2016). However, recent studies have reported that dopaminergic axons projecting to the TS did not respond to the reward prediction error, but exhibited strong excitation in response to novel cues and aversive stimuli as measured using optical fiber fluorometric recording of bulk calcium signals (Eshel et al., 2016; Menegas et al., 2017; Menegas et al., 2018). Anatomically, the TS receives inputs preferentially from the auditory, visual, somatosensory, and gustatory cortices, whereas the other striatal areas receive inputs from multiple other cortical regions (Hannicutt et al., 2016; Jiang and Kim. 2018; Hintiryan et al., 2016). Moreover, dopaminergic neurons projecting to the TS preferentially receive inputs from the GP, while those projecting to the other striatal areas preferentially receive inputs from the ventral striatum (Menegas et al., 2015). These studies suggest that the TS has distinct dopamine inputs, neural circuits, and functions from those of the other striatal areas.

1. 4. The tail of the caudate nucleus in primates

In primates, the striatum is developmentally divided into two parts—the putamen and the caudate nucleus. The caudate nucleus is divided into three subregions—the head of the caudate nucleus (CDh), the caudate body, and the tail of the caudate nucleus (CDt)—and these regions are delineated by the

anterior commissure (head-body) and the genu (body-tail) (Kim and Hikosaka, 2013). The TS in rodents is thought to correspond to the CDt in primates. In primates as well as rodents, some dopaminergic neurons are known to transmit additional non-reward signals related to surprising, novel, salient, and even aversive experiences (Redgrave et al., 1999; Horvitz et al., 1997; Horvitz, 2000; Di Chiara, 2002; Joseph et al., 2003; Pezze and Feldon, 2004; Lisman and Grace, 2005; Redgrave and Gurney, 2006; Shultz et al., 2015; Kim et al., 2015). Kim and colleagues have reported that, unlike the dopaminergic neurons projecting to the CDh, those projecting to the CDt do not respond to the reward prediction error (Kim et al., 2015). They also revealed that single caudate neurons encode the values of visual objects in a regionally distinct manner. CDh neurons encode flexible value learning values of visual objects quickly and flexibly, whereas CDt neurons encode stable value learning object values slowly but retain them longer (Kim and Hikosaka, 2013; Kim and Hikosaka, 2015). Differences in neural circuits between the CDh and the CDt were also demonstrated. The CDh and the CDt receive inputs from distinct cortical regions, subcortical regions, and topographically separate groups of dopamine neurons in the SNc (Kim et al., 2014; Kim & Hikosaka, 2015; Hikosaka et al., 2017). CDh-projecting neurons are located in the rostral-ventral-medial region of the SN, while CDt-projecting neurons are located in the caudal-dorsolateral region (Kim et al., 2014). As mentioned previously, the TS in rodents is thought to correspond to the CDt in primates; however, it remains unknown whether the D1R- and D2R-poor zones in the TS in rodents are also conserved in the CDt in primates.

1. 5. Research aims

The aim of this research was to elucidate the presence of the D1R- and D2R-poor zones in rodents using endogenous dopamine receptors, anatomically characterize these distinct subregions, identify whether the D1R- and D2R-poor zones are conserved in primates, and clarify where MSNs in the D1R- and D2R-poor zones project to. The findings of this research may help understand how the D1R- and D2R poor zones in the TS are anatomically organized and whether they truly represent unique subregions of the striatum. As studies on the output structure of the D1R- and D2R-poor zones are lacking, understanding the differences in output targets among the D1R-poor zone, the D2R-poor zone, and the other striatal areas would be key to elucidating why the TS and the other striatal areas function differently. In addition, by comparing the location of the D1R- and D2R-poor zones in rodents with those in primates, their relative positions in the striatum of rodents and primates could be determined. This finding will help bridge the gap between research on the striatum in rodents and primates.

Chapter 2. Materials and methods

All animal experiments in mice and rats were approved and performed in accordance with the guidelines for the care and use of laboratory animals established by the Committee for Animal Care and Use and that for Recombinant DNA Study of Doshisha University. All animal experiments in marmosets were conducted in accordance with experimental procedure protocols approved by the Animal Welfare and Animal Care Committee of the Primate Research Institute of Kyoto University. All possible efforts were made to minimize animal suffering and the number of animals used.

2. 1. Tissue processing for immunohistochemistry in mice and rats

Male mice (C57BL/6J, 8–13 weeks old, N = 21; C57BL/6J, 3 weeks old, N = 3; ICR, 8 weeks old, N = 3) and male rats (Long-Evans, 10 weeks old, N = 3; Wistar, 10 weeks old, N = 3) were deeply anesthetized using sodium pentobarbital (100 mg/kg, i.p.; Kyoritsu Seiyaku Corporation, Tokyo, Japan). Thereafter, the mice and rats were transcardially perfused with 8.5% sucrose in 20 mM phosphate buffer (PB) containing 1 mM $MgCl_2$, and then with 4% w/v formaldehyde and 75% saturated picric acid in 0.1 M PB. After perfusion, the bodies were left with the fixative for in situ post-fixation for 1.5 h at room temperature (RT), after which the brain was removed from the skull and immersed in 30% sucrose in phosphate-buffered saline (PBS) for 48 h at 4°C for cryoprotection. Tissue blocks were sectioned sagittally or coronally using a freezing microtome (Leica Microsystems, Wetzlar, Germany) at a thickness of 20 or 25 μm. Serial sections were collected and stored in 0.1 M

PB containing 0.02% of sodium azide until further use. Thereafter, sections were incubated overnight at RT with the appropriate primary antibodies (Table 1) diluted in antibody incubation buffer (AIB) containing 10% (v/v) normal donkey serum (Merck KGaA, Darmstadt, Germany), 2% bovine serum albumin, and 0.5% (v/v) Triton X-100 in 0.05 M Tris-buffered saline (TBS), pH 7.4. After the incubation, the sections were washed in PBS and incubated for 3–4 h at RT in AIB containing the appropriate fluorophore-conjugated secondary antibodies (Table 2). After washing, the sections were mounted onto glass slides, air dried, and cover-slipped with 50% (v/v) glycerol/TBS. Immunofluorescence was observed under an epifluorescence microscope (BZ-X710; Keyence, Osaka, Japan and BX-61; Olympus, Tokyo, Japan) or a confocal microscope (FV1200, Olympus). Images from each channel were obtained sequentially, but not simultaneously, to minimize bleed-through.

Table 1. Primary antibodies used for research purposes

Antigen	Host Species	Dilution	Supplier	Catalog no.
Alexa Fluor 488	Rabbit	1:2000	Thermo Fisher Scientific, Inc. (Waltham, MA, USA)	A11094
Dopamine receptor D1	Guinea pig	1:500	Frontier Institute (Ishikari, Japan)	D1R-GP-Af500
Dopamine receptor D1	Rat	1:100	Sigma Aldrich (St. Louis, MO)	D2944
Dopamine receptor D2	Rabbit	1:500	Frontier Institute	D2R-Rb-Af960
Dopamine receptor D2	Guinea pig	1:200	Frontier Institute	D2R-GP-Af500
Dopamine transporter	Goat	1:1000	Frontier Institute	DAT-Go-Af980
GFP	Rat	1:1000	Nacalai Tesque (Kyoto, Japan)	04404-26
NeuN	Mouse	1:5000	EMD Millipore (Temecula, CA)	MAB377
NeuN	Rabbit	1:5000	Millipore	ABN78
Parvalbumin	Mouse	1:4000	Sigma Aldrich	P3088
PHA-L	Rabbit	1:2000	Vector laboratories (Burlingame, CA, UCA)	AS-2300
Preproenkephalin	Rabbit	1:2000	Neuromics (Edina, MN, USA)	RA14124
Serotonin	Rabbit	1:2000	Sigma Aldrich	S5545
Tyrosine hydroxylase	Mouse	1:2000	Millipore	MAB318

Table 2. Secondary antibodies and fluorophores used in research

Secondary antibody and Fluorophore	Host Species	Dilution	Supplier	Catalog no.
Anti-mouse Alexa Fluor®488	Donkey	1:500	Thermo Fisher Scientific, Inc.	A21202
Anti-mouse Alexa Fluor®546	Donkey	1:500	Thermo Fisher Scientific, Inc.	A10036
Anti-mouse Alexa Fluor®635	Goat	1:500	Thermo Fisher Scientific, Inc.	A31575
Anti-goat Alexa Fluor®633	Donkey	1:500	Thermo Fisher Scientific, Inc.	A21082
Anti-guinea pig Alexa Fluor®488	Donkey	1:500	Jackson Immuno Research Inc. (West Grove, PA, USA)	706-545-148
Anti-guinea pig Alexa Fluor®555	Goat	1:500	Thermo Fisher Scientific, Inc.	A21435
Anti-guinea pig Alexa Fluor®633	Goat	1:500	Thermo Fisher Scientific, Inc.	A21105
Anti-rabbit Alexa Fluor®488	Donkey	1:500	Thermo Fisher Scientific, Inc.	A21206
Anti-rabbit Alexa Fluor®546	Donkey	1:500	Thermo Fisher Scientific, Inc.	A10040
Anti-rabbit Alexa Fluor®635	Donkey	1:500	Thermo Fisher Scientific, Inc.	A31577
Anti-rat Alexa Fluor®350	Goat	1:200	Thermo Fisher Scientific, Inc.	A21093
Anti-rat Alexa Fluor®488	Donkey	1:500	Thermo Fisher Scientific, Inc.	A21208
Biotinylated donkey anti-mouse IgG	Donkey	1:100	Jackson Immuno Research Inc.	715-065-151
Biotinylated donkey anti-rat IgG	Donkey	1:100	Jackson Immuno Research Inc.	715-065-153
CF488-streptavidin		1:1000	Biotium (Fremont, CA)	29034

2. 2. Tissue processing for immunohistochemistry in marmosets

Common marmosets (*Callithrix jacchus*, 5 years and 2 months old or 6 years and 10 months old, N = 2) were used for this study (gifted by Dr. Inoue). Following sedation with ketamine hydrochloride (40 mg/kg, i.m.), the marmosets were deeply anesthetized with an overdose of sodium pentobarbital (50 mg/kg, i.v.) for perfusion-fixation. Thereafter, the marmosets were transcardially perfused with PBS and then 4% paraformaldehyde (PFA) in 0.1 M PB. The brains were removed from the skull, postfixed in fresh fixative overnight, and cryoprotected with 30% sucrose in PB at 4 ˚C. The procedures described so far were carried out by Dr. Inoue at the Primate Research Institute of Kyoto University. Tissue blocks containing the putamen and caudate nucleus were sectioned coronally using a freezing microtome (Leica Microsystems) at a thickness of 25 μm. Serial sections were collected in 0.1 M PB containing 0.02% sodium azide and incubated overnight at RT with the appropriate primary antibodies diluted in AIB (Table 1). After the incubation, the sections were washed in PBS and incubated for 3–4 h at RT in AIB containing the appropriate fluorophore-conjugated secondary antibodies (Table 2). After rinsing, the sections were again incubated overnight at RT with the appropriate primary antibodies, and then washed in PBS and incubated for 3–4 h at RT in the same buffer again. This process was repeated two more times in order to strengthen the signal. After rinsing, the sections were mounted onto glass slides, air dried, and cover-slipped with 50% (v/v) glycerol/TBS.

2. 3. Analysis of immunofluorescence images for D1R and D2R

To visualize the distribution of dopamine receptors from the rostral to the caudal striatum,

immunofluorescence signals along a line was measured using the profile function in ImageJ (v. 1.47). The line was drawn rostro-caudally to cross the middle of the D1R-poor zone and the D2R-poor zone at lateromedial (LM) 3.0 mm and parallel to the boundary between the striatum and the amygdalo-striatal transition area (ASt), and traversed the cortex, striatum, D1R- and D2R-poor zones, and internal capsule (ic). Pixel intensities of triple fluorescent signals in CLSM images (1 pixel = 14.24 μm^2; no signal = 0, maximum level = 255) were measured.

2. 4. Dopamine receptor in situ hybridization and NeuN immunolabeling

Male mice (C57BL/6J, 8–13 weeks old, N = 3) were deeply anesthetized with isoflurane (Pfizer Japan Inc.) and sodium pentobarbital (100 mg/kg, i.p.; Kyoritsu Seiyaku Corporation). Thereafter, the mice were transcardially perfused with 8.5% sucrose in 20 mM PB containing 1 mM $MgCl_2$ and then with 4% w/v PFA in 0.1 M PB. The brain was removed from the skull, postfixed for 72 h at 4 ℃, and then cryoprotected with 30% sucrose in PBS for 48 h at 4 ℃. Tissue blocks were sectioned sagittally using a freezing microtome at a thickness of 20 μm. Serial sections were collected in 0.1 M PB containing 0.1% diethylpyrocarbonate (0.1 M PB-DEPC) and then stored at -20 ℃ in section preservation buffer (30% glycerol, 30% ethylene glycol, 0.34% NaCl, 0.1 M PB, 0.1% diethylpyrocarbonate). In situ hybridization probes were gifted by Mr. Okamoto. To prepare in situ hybridization probes, the complementary DNA fragments for Drd1 (nucleotides 1116-1809; GenBank accession No. NM_010076.3) and Drd2 (nucleotides 1412-2497; GenBank accession No. X55674.1) were cloned separately into the pBSIISK vector. By using the linearized plasmids as template, sense and anti-sense

single-strand RNA probes were synthesized using a digoxigenin (DIG) or fluorescein isothiocyanate (FITC) RNA labeling kit (Roche Applied Science). The procedures described so far were carried out by Mr. Okamoto. Free-floating sections were washed twice for 10 min in 0.1 M PB-DEPC, incubated for 20 min in 0.1 M PB-DEPC containing 0.3% Triton X-100, and then acetylated for 10 min with 0.25% (v/v) acetic anhydride in 0.1 M triethanolamine. After washing twice for 10 min with 0.1 M PB-DEPC, the sections were preincubated for 1 h at 60 °C with a hybridization buffer consisting of 5 x saline sodium citrate (SSC; 1x SSC = 0.15 M NaCl and 0.015 M sodium citrate, pH 7.0), 2% (w/v) blocking reagent (Roche Applied Science), 50% (v/v) formamide, 0.1% (w/v) N-lauroylsarcosine (NLS), and 0.1% (w/v) SDS. Thereafter, the sections were hybridized for 16–20 hours at 60 °C with 1 µg/ml DIG-labeled antisense RNA probe or FITC-labeled antisense RNA probe in the hybridization buffer. After washing twice in 2 x SSC containing 50% (v/v) formamide and 0.1% (w/v) NLS for 20 min at 60 °C, the sections were incubated with 20 µg/ml ribonuclease A (RNase A) for 30 min at 37 °C in 10 mM Tris-HCl (pH 8.0) containing 1 mM ethylenediamine tetraacetic acid and 0.5 M NaCl, followed by two washes with 2 x SSC containing 0.1% (w/v) NLS for 20 min at 37 °C and two additional washes with 0.2 x SSC containing 0.1% (w/v) NLS for 20 min at 37 °C. Sections were then washed for 5 min at RT with 0.1 M TBS pH 7.5 (TS7.5), followed by preincubation with TS7.5 containing 1% blocking reagent. Subsequently, the sections were incubated overnight at RT with 1:1,000-diluted alkaline phosphatase-conjugated sheep anti-DIG antibody (11-093-274-910; Roche Applied Science) to DIG-labeled antisense RNA probe or alkaline phosphatase-conjugated anti-FITC sheep antibody (11-426-338-910; Roche Applied Science) to FITC-labeled

antisense RNA probe in TS7.5 containing 1% blocking reagent. After washing three times for 10 min with 0.1 M TBS pH 9.5 (TS9.5), the sections were reacted for 27–42 hours with 2% 5-bromo-4-chloro-3-indolyl-phosphate (NBT) and nitro blue tetrazolium (BCIP) (Roche #168145) in TS9.5 containing 0.05% Tween 20. Sections were washed three times for 10 min with TS7.5 containing 0.05% Tween-20 (TNT), and then incubated overnight at RT with TNT. For the subsequent NeuN immunolabeling, the sections processed for in situ hybridization were incubated for 20 min with PBS containing 1% H_2O_2 and washed twice for 10 min with PBS containing 0.3% Triton X-100 (PBST). Thereafter, the sections were incubated overnight at RT with mouse anti-NeuN antibody diluted at 1/10000 in AIB. Subsequently, the sections were washed three times for 10 min in PBST and incubated for 3 h with 10 µg/mL biotinylated donkey anti-mouse IgG in PBST, followed by three washes for 10 min with PBS. Then the sections were incubated overnight at 4°C with avidin-biotin-peroxidase complex (ABC; ABC Elite; Vector, Burlingame, CA) in PBST. After rinsing with PBS, the bound peroxidase was detected as a black reaction product by incubation for 2 h in 0.02 % (w/v) diaminobenzidine-4HCl (DAB) and 0.001 % (v/v) H_2O_2 in 50 mM Tris–HCl, pH 7.6. This long incubation was necessary to make NeuN immunolabeling distinct enough over the background and the NBT/BCIP signals from in situ hybridization. The reaction was terminated by rinsing the sections with PBS containing 2 % (w/v) sodium azide, followed by two rinses in PBS. The stained sections were serially mounted onto gelatinized glass slides, dried, washed in running water, dried again, cleared in xylene, and finally covered with mounting medium MX (Matsunami; Kishiwada, Japan) and glass coverslips.

2. 5. Quantification of striatal neurons expressing either D1R or D2R mRNA

To investigate the cell composition of the D1R- and D2R-poor zones, we analyzed the proportions of D1R- and D2R-expressing neurons in different areas of the striatum. Brain sections processed for the detection of D1R mRNA by in situ hybridization and the neuronal marker NeuN with DAB by immunohistochemistry were used for the analysis. We counted the cells positive for either D1R or D2R mRNA and NeuN immunolabeling and computed the proportion of neurons expressing the dopamine receptors out of all neurons in four different areas: the rostral part of the DS (rDS), the caudal part of the DS (cDS), the D1R-poor zone, and the D2R-poor zone. To define the boundaries of the D1R-poor zone, the D2R-poor zone, and the other striatal areas, we used double immunofluorescent staining for D1R and D2R in the sections adjacent to the section in which we performed in situ hybridization. The data for the four subregions were statistically compared using one-way analysis of variance (ANOVA) and the Tukey-Kramer test in MATLAB (R2019b).

2. 6. AAV injection in TH-Cre mouse

Male TH-Cre mice (22 weeks old, N = 2) were anesthetized by inhalation of isoflurane followed by intramuscular injection of a mixture of ketamine (Ketalar; Daiichi-Sankyo, Tokyo, Japan; 40 mg/kg) and xylazine (Bayer HealthCare, Tokyo, Japan; 4 mg/kg). Each mouse was then fixed to a stereotaxic device (Narishige, Tokyo, Japan), and a small hole was drilled at an appropriate position in the skull in accordance with the mouse brain atlas (Paxinos and Watson 2013). For dopaminergic neuron axon labeling, 0.3 μL of a viral vector (1.5 x 1010 vg/μL adeno-associated virus (AAV)-Efla-DIO-EGFP;

Addgene plasmid # 37084) was injected into the SNc of TH-Cre transgenic mice [anteroposterior (AP): 3.0 mm caudal to the bregma, LM: 1.6 mm lateral from the midline, depth: 3.8 mm from the pial surface] using a glass pipette (tip diameter, 20–30 μm) through which air pressure pulses were delivered using a pressure injector (PV820; World Precision Instruments, Sarasota, FL, USA). Each mouse was perfused with 8.5% sucrose in 20 mM PB containing 1 mM $MgCl^2$, and then with 4% w/v formaldehyde and 75% saturated picric acid in 0.1 M PB at least 2 weeks after AAV injection. For the subsequent GFP immunolabeling, the sections were incubated for 20 min with PBS containing 1% H_2O_2 and washed twice for 10 min with PBST. Thereafter, the sections were incubated overnight at RT with rat anti-GFP antibody diluted at 1/1000 in AIB, washed three times for 10 min in PBST, incubated for 3 h with 10 μg/mL biotinylated donkey anti-rat IgG in PBST, and then washed thrice for 10 min each with PBS. Subsequently, the sections were incubated overnight at 4 ℃ with ABC in PBST. After rinsing with PBS, the bound peroxidase was detected as a black reaction product by incubation for 7 min in 0.02 % (w/v) DAB and 0.001 % (v/v) H_2O_2 in 50 mM Tris–HCl, pH 7.6. The reaction was terminated by rinsing the sections with PBS containing 2 % (w/v) sodium azide, followed by two rinses in PBS. The stained sections were serially mounted onto gelatinized glass slides, dried, washed in running water, dried again, cleared in ethanol and then xylene, and finally covered with mounting medium MX and glass coverslips.

2. 7. Retrograde tracer injection into the output nuclei of the basal ganglia

Male mice (C57BL/6J, 10–13 weeks old, N = 4) were prepared for injection as described above. For

dMSN labeling, 0.5 µl of 1% cholera toxin subunit B – Alexa Fluor 555 conjugate (CTB555) (C22843, Thermo fisher Scientific, Inc.) in 0.1 M PB was injected into the entire output nuclei of the basal ganglia using a glass pipette (tip diameter, 15–20 µm) through which air pressure pulses were delivered using a pressure injector (PV820; World Precision Instruments, Sarasota, FL, USA). The main target of injection was the SN [AP: 2.8 mm caudal to the bregma, LM: 2.1 mm lateral from the midline, depth: 3.7-4.2 mm from the pial surface]. The site of injection extended to the SNr, SNc, and EP, but not the GP, because iMSNs project to the GP. Each mouse was perfused 3 or 4 days after the tracer injection, and tissues were prepared for immunofluorescence labeling as described above. To define the boundaries of the D1R-poor zone, the D2R-poor zone, and other striatal areas, we used double immunofluorescence staining for D1R and D2R in sections adjacent sections to those used for counting labeled neurons. To confirm that retrogradely labeled neurons expressed D1R mRNA but not D2R mRNA, we also injected 0.5 µl of 1% CTB conjugated with Alexa Fluor 488 (CTB488) in 0.1 M PB into the entire output nuclei of the basal ganglia using a glass pipette (tip diameter, 15–20 µm) through which air pressure pulses were delivered using a pressure injector. Brain sections processed for the detection of D1R mRNA by in situ hybridization and anti-Alexa Fluor 488 antibody with DAB by immunohistochemistry were used for the analysis. To confirm the density of dMSNs in the D1R- and D2R-poor zones, we counted and computed the retrogradely labeled dMSNs in four different areas: the rDS, cDS, the D1R-poor zone, and the D2R-poor zone. The data for the four subregions were statistically compared using one-way ANOVA and the Tukey-Kramer test in MATLAB.

2. 8. Anterograde tracer injection into the D1R-poor zone, the D2R-poor zone, and the caudal dorsal striatum

Male mice (C57BL/6J, 8–13 weeks old, N = 4) were prepared for injection as described above. 10% biotinylated dextran amine (BDA) (D1956, Invitrogen) in PBS was injected into the D1R- and/or D2R-poor zones (AP: 1.1 mm caudal to the bregma, LM: 3.4 mm lateral from the midline, depth: 3.3 mm from the pial surface) using a glass pipette (tip diameter, 15–20 μm). Since the difference between the coordinates of the D1R-poor zone and D2R-poor zone was slight, we used the individual differences of mice to inject the tracer in two different locations using a single coordinate. The BDA solution was injected iontophoretically into one site per animal using a 1.2 μA pulse current (7 s on and 7 s off) for 5–20 min. Each mouse was perfused 3 or 4 days after the tracer injection, and tissues were prepared for immunolabeling as described above. Male mice (C57BL/6J, 13 weeks old, N = 3) were prepared for injection as described above. *Phaseolus vulgaris* leucoagglutinin (PHA-L) (L-1110, Vector Laboratories) (2.5% in 10 mM phosphate, pH 8.0) was injected into the caudal dorsal striatum (AP: 1.1 mm caudal to the bregma, LM: 3.4 mm lateral from the midline, depth: 2.5 mm from the pial surface) near the D1R- and D2R-poor zones using a glass pipette (tip diameter, 20–25 μm). The PHA-L solution was injected iontophoretically into one site per animal using a 4 μA pulse current (7 s on and 7 s off) for 5 min. Each mouse was perfused 5 days after the tracer injection, and tissues were prepared for immunolabeling as described above.

2. 9. Analysis of axon distribution from striatal neurons in the D1R- and D2R-poor zones and the caudal dorsal striatum to the SN

BDA-positive and PHA-L-positive axons were selected objectively using the following procedure and ImageJ: (1) the original images were acquired using epifluorescence microscope (MFM); (2) after inversion of gray levels in each image (no signal = 0, maximum level = 255); (3) background signals were subtracted via the "Rolling Ball" command in ImageJ; (4) images were thresholded at a constant gray level for each channel to obtain binary images; and (5) image tilts were adjusted using the midline of the brain (Fig. 2). The boundary of the SNL was delineated by immunoreactivities for TH and NeuN, because the SNL is known to have a low density of neurons; the dopaminergic neurons of the SNL are located apart from those of the SNc, and dopaminergic fibers are distributed within the SNr like the inverted letter C of the alphabet and sparse at the boundary between the SNL and the SNr. The contours of four subregions—the dSNL, vSNL, dlSNr, and vlSNr—were plotted objectively in Adobe Photoshop using the following procedure: (1) the original fluorescence images for BDA and TH were acquired using MFM; (2) the boundary of the SNL was applied to the fluorescence images for BDA and TH; (3) the boundary between the dSNL and vSNL was drawn as a bisector between the top and the bottom of the SNL; (4) the boundary between the dlSNr and vlSNr was drawn at the bottom line of the vSNL and at the perpendicular bisector of width in the SNr, excluding for SNc; (5) the boundaries between four subregions were applied to the binary images. To statistically confirm the bias of axon distribution, we counted the black pixels of binary images using Adobe Photoshop, and computed the proportion of number of pixels among the dSNL, vSNL, dlSNr, and vlSNr. The

data for the four subregions were statistically compared using one-way ANOVA and the Tukey-Kramer test in MATLAB.

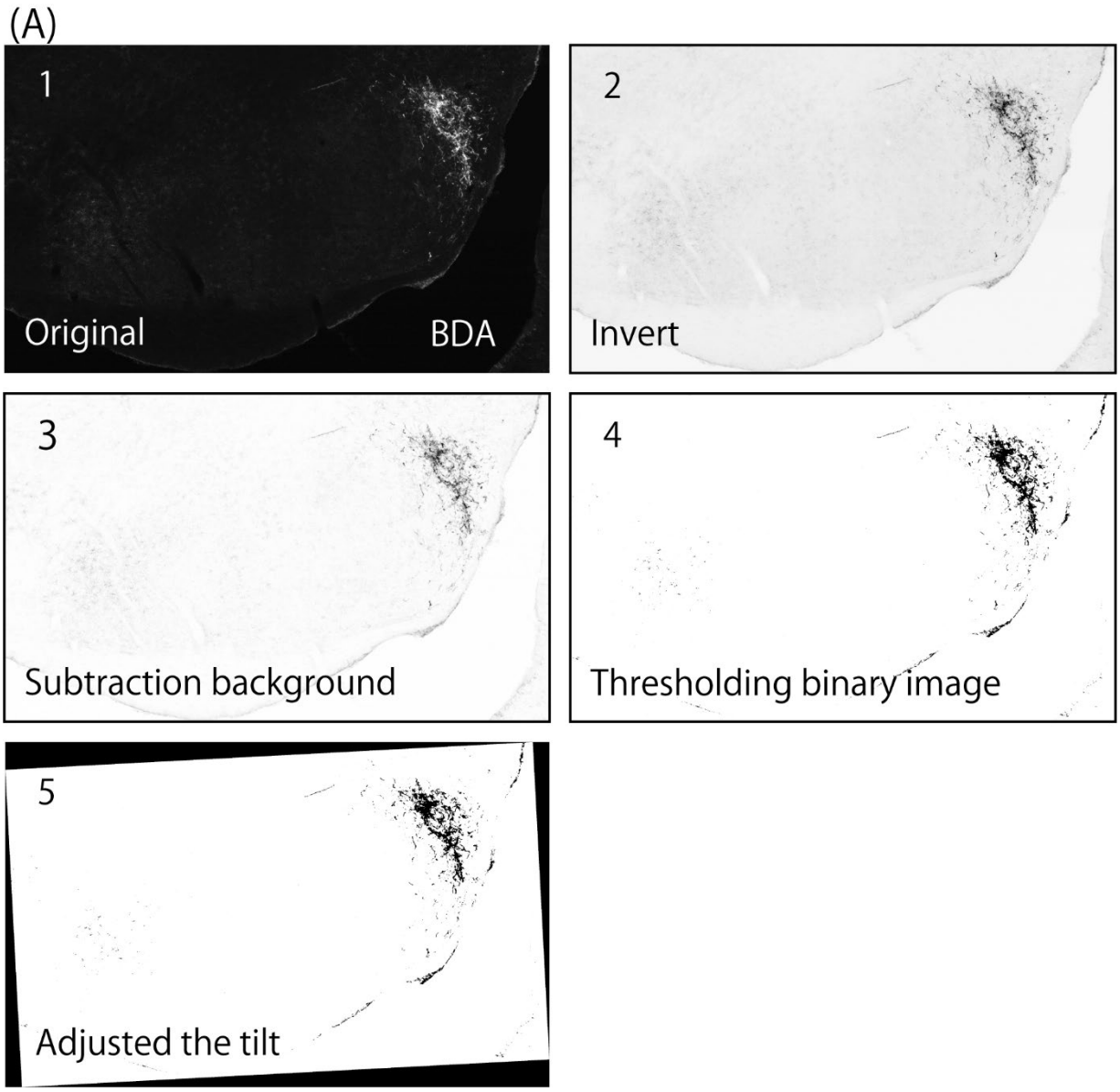

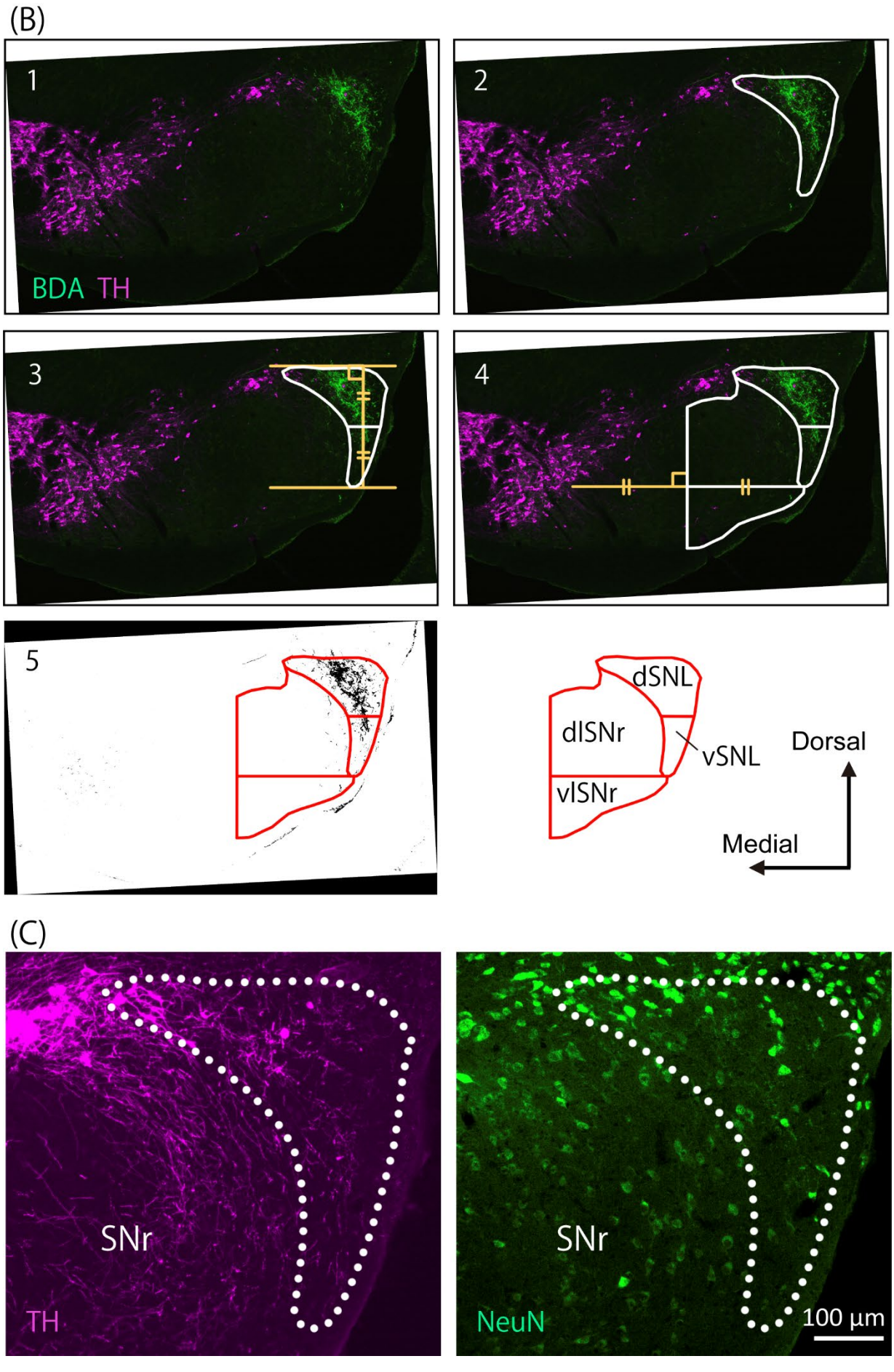
(B)
1
BDA TH
2
3
4
5
dSNL
dlSNr
vSNL
vlSNr
Dorsal
Medial
(C)
SNr
TH
SNr
NeuN
100 μm

Fig. 2 Procedure for binary imaging and subdivision of the substantia nigra (SN)

(A-1) The original fluorescence image for biotinylated dextran amine (BDA) (white) was acquired using MFM. (A-2) Inversion image of gray levels in an image (no signal = 0, maximum level = 255). (A-3) Image of subtracted background signals. (A-4) Binary image obtained by thresholding the image at a constant gray level for each channel. (A-5) Image tilt adjusted using the midline of the brain. (B-1) The original fluorescence image for BDA (green) and TH (magenta) acquired using MFM. (B-2) The boundary of the substantia nigra pars lateralis (SNL) delineated in panel C was applied to the fluorescence image in panel B-1. (B-3) The boundary between the dSNL and vSNL, drawn as a bisector between the top and the bottom of the SNL. (B-4) The boundary between the dlSNr and vlSNr, drawn at the bottom line of the vSNL and at the perpendicular bisector of width in the SNr, excluding the SNc. (B-5) The boundaries among the four subregions applied to the binary image. (C) The boundary of the SNL was delineated by immunoreactivities for TH (magenta) and NeuN (green). The white dotted lines indicate the contour of the SNL.

Chapter 3. Results

3. 1. Distinct subregions in the mouse caudal lateral striatum

The presence of D1R- and D2R-poor zones has previously been shown using transgenic animals expressing fluorescent proteins or tagged proteins in the respective neuronal populations (Gangarossa et al., 2013; Miyamoto et al., 2018). Follow-up studies have also quantitatively analyzed the distinctive neuronal populations in each zone using transgenic mice (Miyamoto et al., 2019). However, it remained unclear whether the D1R- and D2R-poor zones could also be defined with the genuine expression of endogenous dopamine receptors, not transgenes. In the present study, we combined immunofluorescence staining and in situ hybridization to detect endogenous receptors and to confirm these subregions in wild-type mice. Double immunofluorescence staining for D1R and D2R in C57BL/6 mice demonstrated the presence of the D1R- and D2R-poor zones in the caudal lateral striatum (Fig. 3-4). The D1R-poor zone extended from 1.10 mm to 2.00 mm posterior to the bregma and from 2.85 mm to 3.30 mm lateral from the midline (Fig. 4). The D2R-poor zone was located lateral to the GP and extended from 1.30 mm to 1.80 mm posterior to the bregma and from 2.70 mm to 3.15 mm lateral from the midline in accordance with the mouse brain atlas (Paxinos and Watson 2007) (Fig. 3B, 4). It is notable that the D1R- and D2R-poor zones are located in the TS reported by Menegas and colleagues (Menegas et al., 2015).

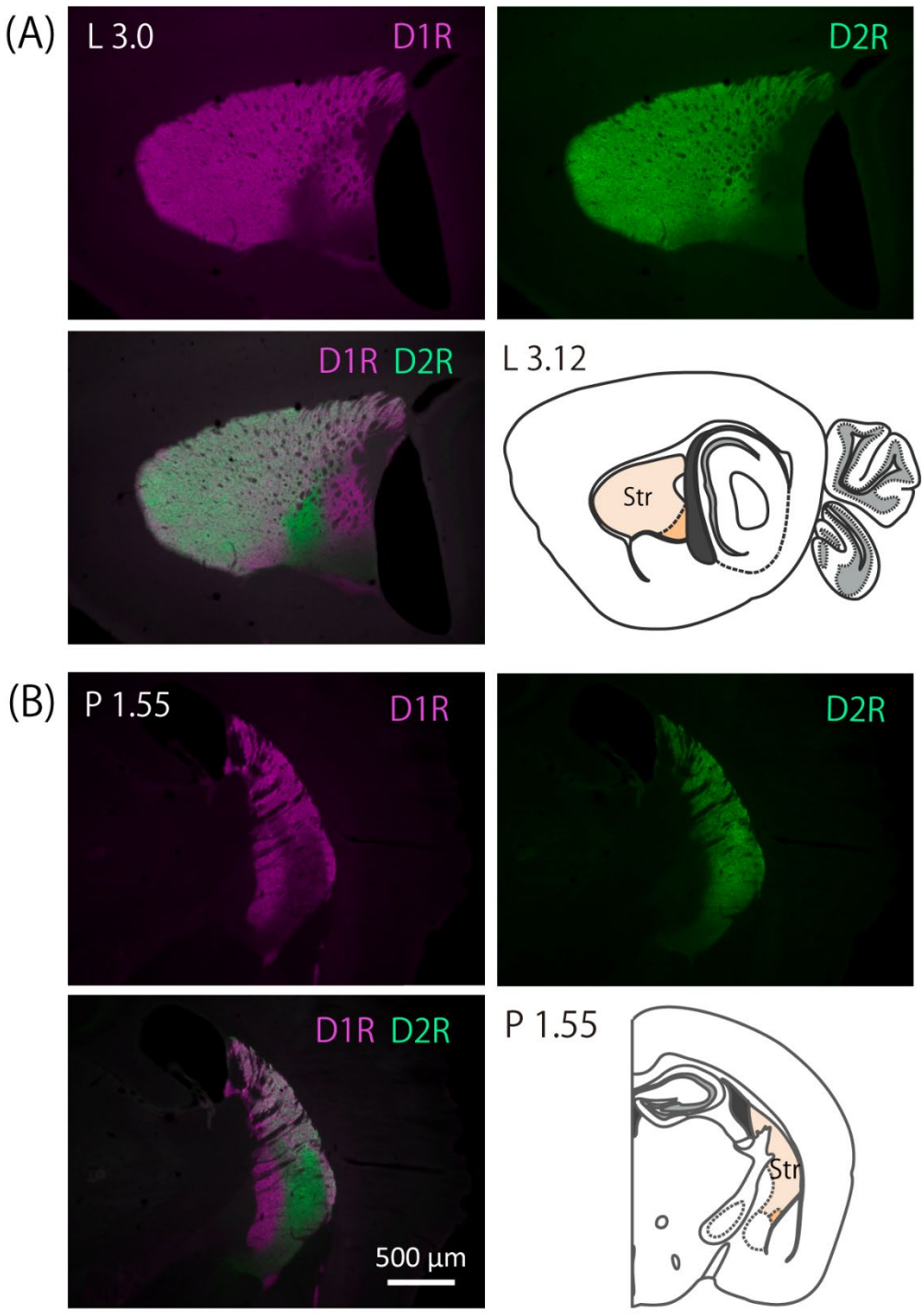

Fig. 3 Distribution of immunoreactivities for dopamine receptor D1 (D1R) and D2 (D2R) in the mouse caudal lateral striatum

(A) Double immunofluorescence labeling for D1R (magenta) and D2R (green) in a sagittal section [at 3.0 mm lateral from the midline (L 3.0)]. Right lower panel shows the atlas image in a sagittal section (L 3.12). The striatum (Str) is shown in light orange and the amygdalo-striatal transition area (ASt) is shown in dark orange. (B) Double immunofluorescence labeling for D1R and D2R in a coronal section [at 1.55 mm posterior to the bregma (P 1.55)]. Note that the D1R-poor zone and the D2R-poor zone are next to each other. Right lower panel shows the atlas image in a coronal section of the right hemisphere (P 1.55). The Str is shown in light orange and the ASt is shown in dark orange.

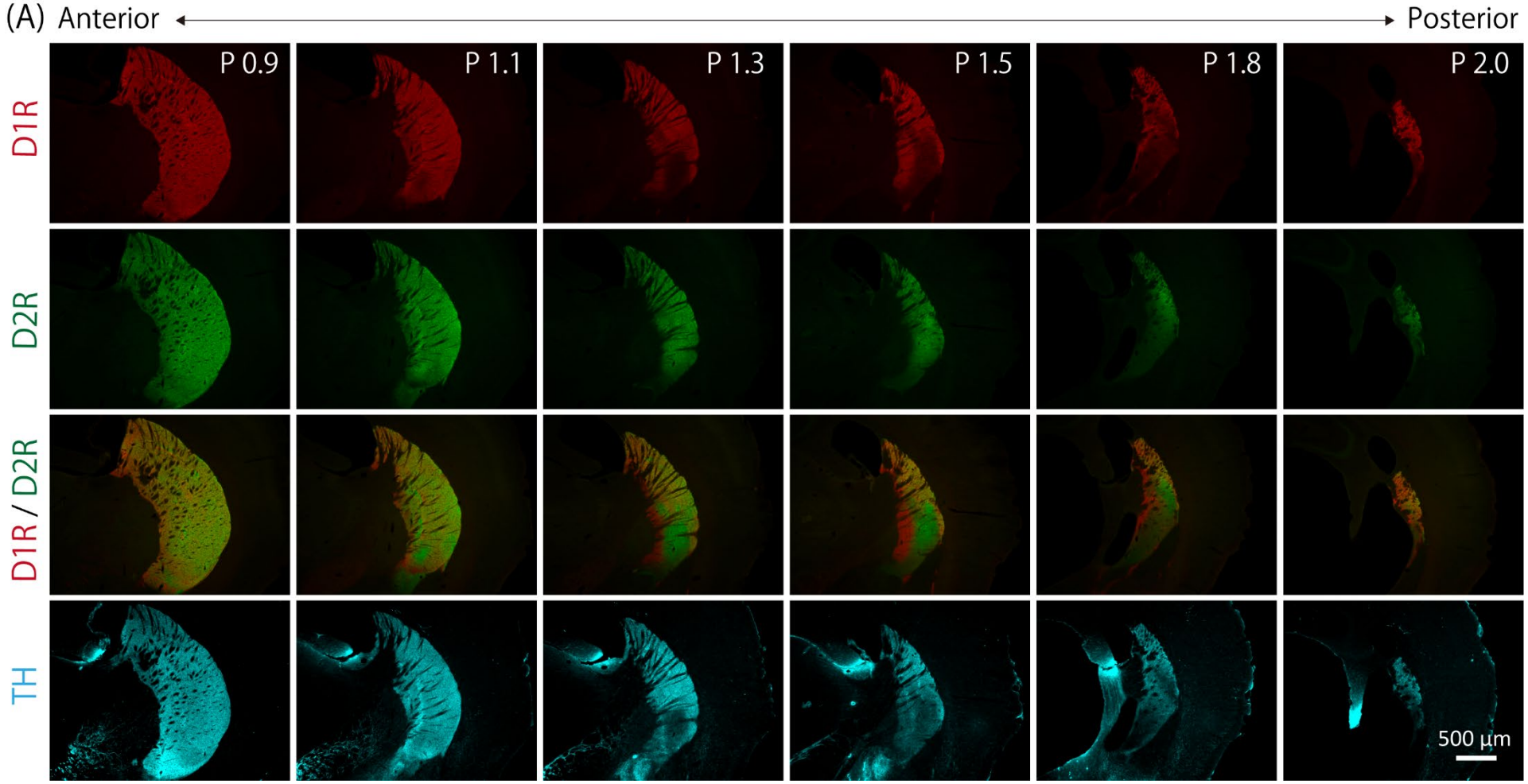
(A) Anterior
Posterior
P 0.9
P 1.1
P 1.3
P 1.5
P 1.8
P 2.0
D1R
D2R
D1R / D2R
TH
500 μm

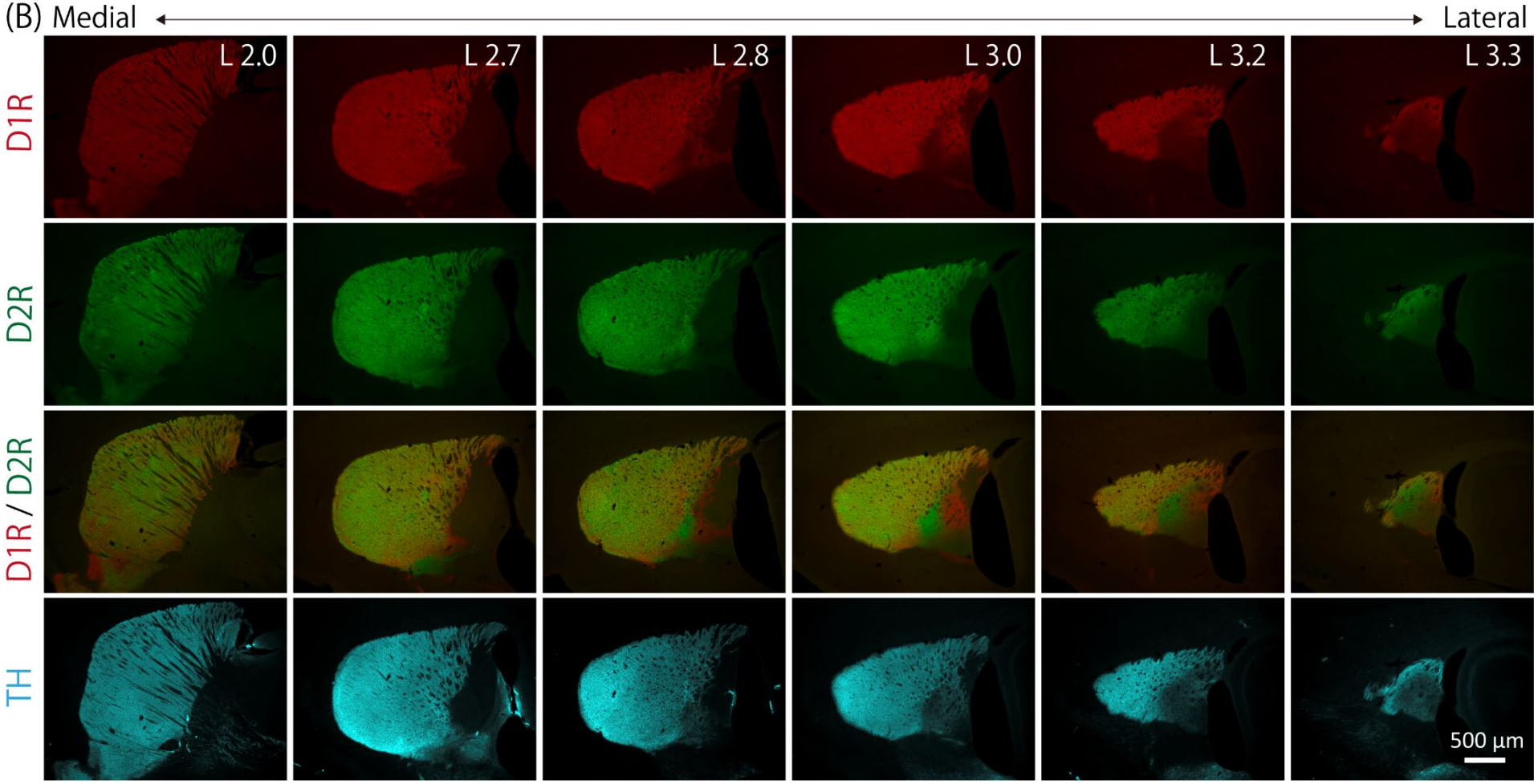
(B) Medial
Lateral
L 2.0
L 2.7
L 2.8
L 3.0
L 3.2
L 3.3
D1R
D2R
D1R / D2R
TH
500 µm

Fig. 4 Spatial distribution of immunoreactivities for D1R, D2R, and tyrosine hydroxylase (TH) in mice

(A) Triple immunofluorescence images for D1R (red), D2R (green), and TH (cyan) in the coronal view [sections from 0.9 mm to 2.0 mm posterior to the bregma (P 0.9–2.0)]. (B) Triple immunofluorescence images for D1R, D2R, and TH in the sagittal view [sections from 2.0 mm to 3.3 mm lateral from the midline (L 2.0–3.3)]. The D1R-poor zone extended from 1.10 mm to 2.00 mm posterior to the bregma and from 2.85 mm to 3.30 mm lateral to the midline. The D2R-poor zone was located lateral to the GP and extended from 1.30 mm to 1.80 mm posterior to the bregma and from 2.70 mm to 3.15 mm lateral to the midline. The D1R- and D2R-poor zones are next to each other. The immunoreactivity for TH was poor in both the D1R-poor zone and the D2R-poor zone.

However, it was difficult to identify individual neurons in immunolabeling for cell population analyses, because dopamine receptors are distributed not only in the somata of MSNs but also in their dendrites and presynaptic terminals innervating onto them, and D2R is also present in cholinergic interneurons (Kreitzer, 2009). Therefore, we performed in situ hybridization of dopamine receptor mRNAs (Drd1 and Drd2) with immunolabeling of the overall neuronal population using a neuronal maker, NeuN. As shown in Fig. 5, in situ hybridization clearly labeled the somata of NeuN-positive neurons expressing the dopamine receptors. This clear immunolabeling of somatic mRNAs and NeuN allowed us to accurately quantify the neuronal densities and the proportions of neurons expressing D1R mRNA and D2R mRNA in different subregions of the caudal lateral striatum. We found that there were no statistically significant differences among the overall neuronal densities of the rDS, cDS, D1R-poor zone, and D2R-poor zone in the caudal lateral striatum (Fig. 5G) (one-way ANOVA, $p = 0.14$, N = 6 sections from three mice). However, the proportions of neurons expressing D1R mRNA and D2R mRNA differed significantly among these regions. The proportion of NeuN+ neurons expressing D1R mRNA was significantly lower in the D1R-poor zone (12.23 ± 1.43%, Tukey-Kramer test, **: $p < 0.01$; D1R-poor zone vs rDS, $p = 5.1\times10^{-8}$; D1R-poor zone vs cDS, $p = 8.1\times10^{-8}$), whereas this proportion was significantly higher in the D2R-poor zone (82.06 ± 3.08%, Tukey-Kramer test, **: $p < 0.01$; D2R-poor zone vs rDS, $p = 1.4\times10^{-7}$; D2R-poor zone vs cDS, $p = 7.1\times10^{-8}$) than those in both DS regions (50.44 ± 0.07% in rDS, 46.49 ± 1.34% in cDS, N = 3 sections from three mice) (Fig. 5C). Conversely, the proportion of NeuN+ neurons expressing D2R mRNA was significantly lower in the D2R-poor zone (3.58 ± 1.19%, Tukey-Kramer test, **: $p < 0.01$; D1R-

poor zone vs rDS, $p = 7.6\times10^{-6}$; D1R-poor zone vs cDS, $p = 7.5\times10^{-6}$), whereas it was significantly higher in the D1R-poor zone (78.68 ± 1.73%, Tukey-Kramer test, **: $p < 0.01$; D2R-poor zone vs rDS, $p = 7.4\times10^{-7}$; D2R-poor zone vs cDS, $p = 7.4\times10^{-7}$) than that in both DS regions (46.78 ± 4.23% in rDS, 46.73 ± 4.13% in cDS, N = 3 sections from three mice) (Fig. 5F). No significant difference was observed between the rDS and cDS in terms of the proportions of either D1R or D2R mRNA expressing neurons (Tukey-Kramer test; rDS vs cDS in D1R mRNA, $p = 0.13$; rDS vs cDS in D2R mRNA, $p = 0.99$). In summary, only 12.2% of the D1R-poor zone neurons were D1R mRNA+ and 78.7% were D2R mRNA+, whereas only 3.6% of the D2R-poor zone neurons were D2R mRNA+ and 82.1% were D1R mRNA+. In the rDS, 50.4% of the neurons were D1R mRNA+ and 46.8% were D2R mRNA+; in the cDS, 46.7% of neurons were D1R mRNA+ and 46.7% were D2R mRNA+ (Fig. 5H). Our results of the cell composition in the D1R- and D2R-poor zones were approximately consistent with the those of the study that used transgenic mice expressing D1R-DARPP-32-Flag/D2R-DARPP-32-Myc (Miyamoto et al., 2019).

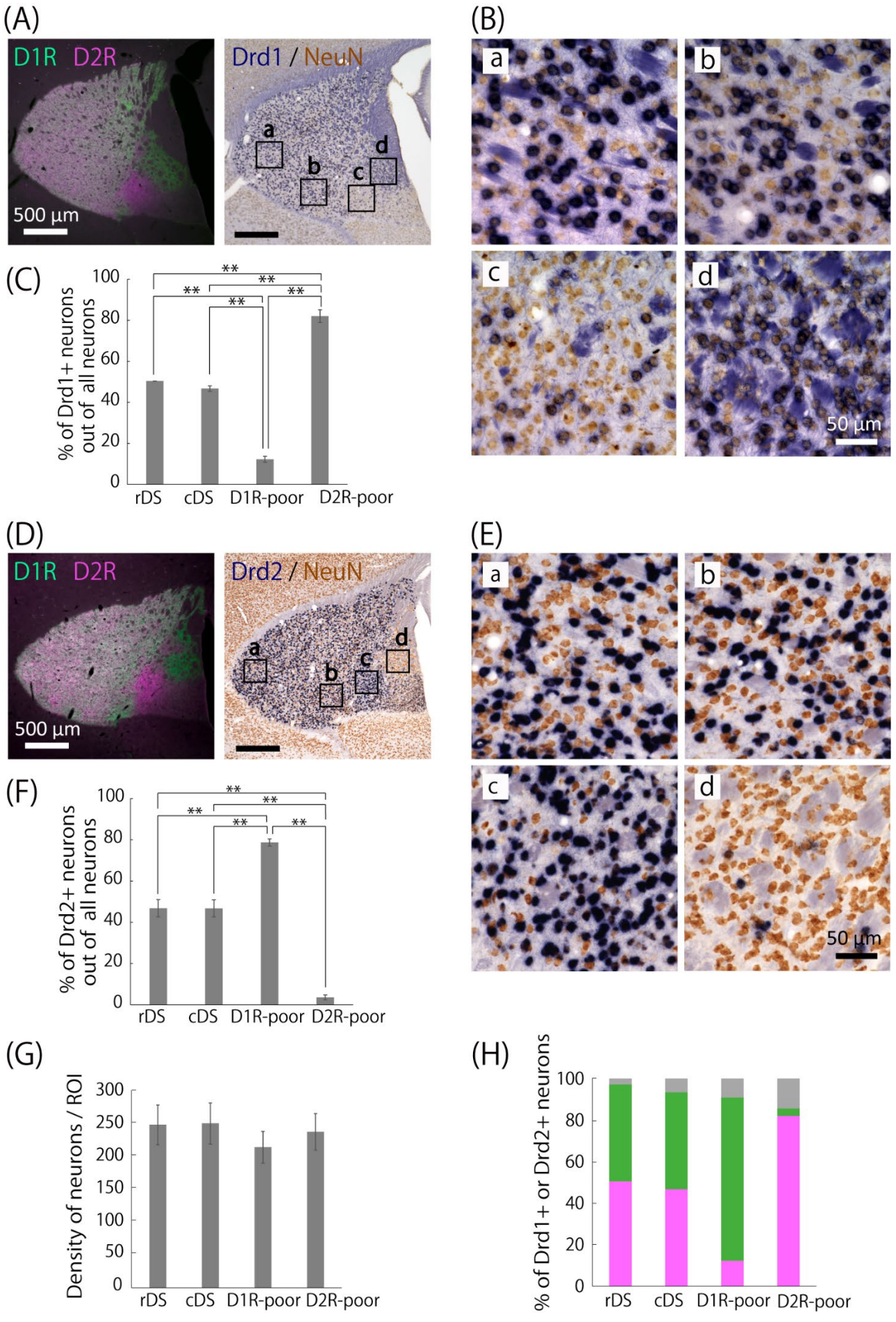
(A)
D1R D2R
500 µm
Drd1 / NeuN
a
b
c
d
(B)
a
b
c
d
50 µm
(C)
% of Drd1+ neurons out of all neurons
100
80
60
40
20
0
**
rDS
cDS
D1R-poor
D2R-poor
(D)
D1R D2R
500 µm
Drd2 / NeuN
(E)
50 µm
(F)
% of Drd2+ neurons out of all neurons
(G)
Density of neurons / ROI
300
250
200
150
100
50
0
(H)
% of Drd1+ or Drd2+ neurons

Fig. 5 Distribution of neurons expressing D1R mRNA and D2R mRNA in four different areas in the mouse caudal lateral striatum

(A) Overlay of immunofluorescence images for D1R (green) and D2R (magenta) (left panel). Double labeling for D1R mRNA by in situ hybridization (dark purple) and NeuN by immunohistochemistry (brown) (right panel). (B) High-magnification images of the four different areas in panel A [the rostral part of the dorsal striatum (rDS) (a), the caudal part of the dorsal striatum (cDS) (b), D1R-poor zone, and (c) D2R-poor zone (d).] (C) The quantification of the proportion of Drd1+ neurons out of NeuN+ neurons in the four different areas (**$p < 0.01$, 3 sections, 1 section/animal). Note that the proportion was significantly lower in the D1R-poor zone than in the DS, but significantly higher in the D2R-poor zone than in the DS. (D) Overlay of immunofluorescence images for D1R (green) and D2R (magenta) (left panel). Double labeling for D2R mRNA by in situ hybridization (dark purple) and NeuN by immunohistochemistry (brown) (right panel). (E) High-magnification images of the four different areas in panel D [rDS (a), cDS (b), D1R-poor zone, and (c) D2R-poor zone (d).] (F) The proportion of Drd2+ neurons out of NeuN+ neurons in the four different areas (**$p < 0.01$, 3 sections, 1 section/animal). Note that the proportion was significantly higher in the D1R-poor zone than in the DS, but significantly lower in the D2R-poor zone than in the DS. (G) The density of NeuN+ neurons in the four different areas (region of interest size: 73711 μm^2, 6 sections, 1 section/animal). (H) The proportion of Drd1+ neurons (pink) and Drd2+ neurons (green) out of NeuN+ neurons in the four different areas (6 sections, 1 section/animal).

3. 2. Sparse dopaminergic axons in the mouse caudal lateral striatum

Previous studies reported that the D1R- and D2R-poor zones exhibit substantially lower immunoreactivity for TH than the other striatal areas (Miyamoto et al., 2019), indicating sparse innervation of dopaminergic neurons. We confirmed this finding with TH immunolabeling—both the D1R- and D2R-poor zones exhibit low immunoreactivity for TH (Fig. 6A-B). In contrast, the immunoreactivity for TH was high and dopamine receptors were densely distributed throughout the dorsal striatum (Fig. 4). The TH-poor area extended from -1.10 mm to -2.00 mm posterior to the bregma and from 2.70 mm to 3.30 mm lateral from the midline (Fig. 4). We also confirmed that the immunoreactivity for the dopamine transporter (DAT) was also poor in these subregions (Fig. 6C). To quantify the intensity of immunoreactivities for D1R, D2R, and TH, we analyzed the pixel intensities in immunofluorescence images along a line traversed the cortex, the striatum, the D1R- and D2R-poor zones, and the ic (Fig. 6D–E). The pixel intensity for D1R was low, but that for D2R was high in the D1R-poor zone. Conversely, the pixel intensity for D2R was low, but that for D1R was high in the D2R-poor zone. The pixel intensity for TH was low in both the D1R-poor zone and the D2R-poor zone (Fig. 6E).

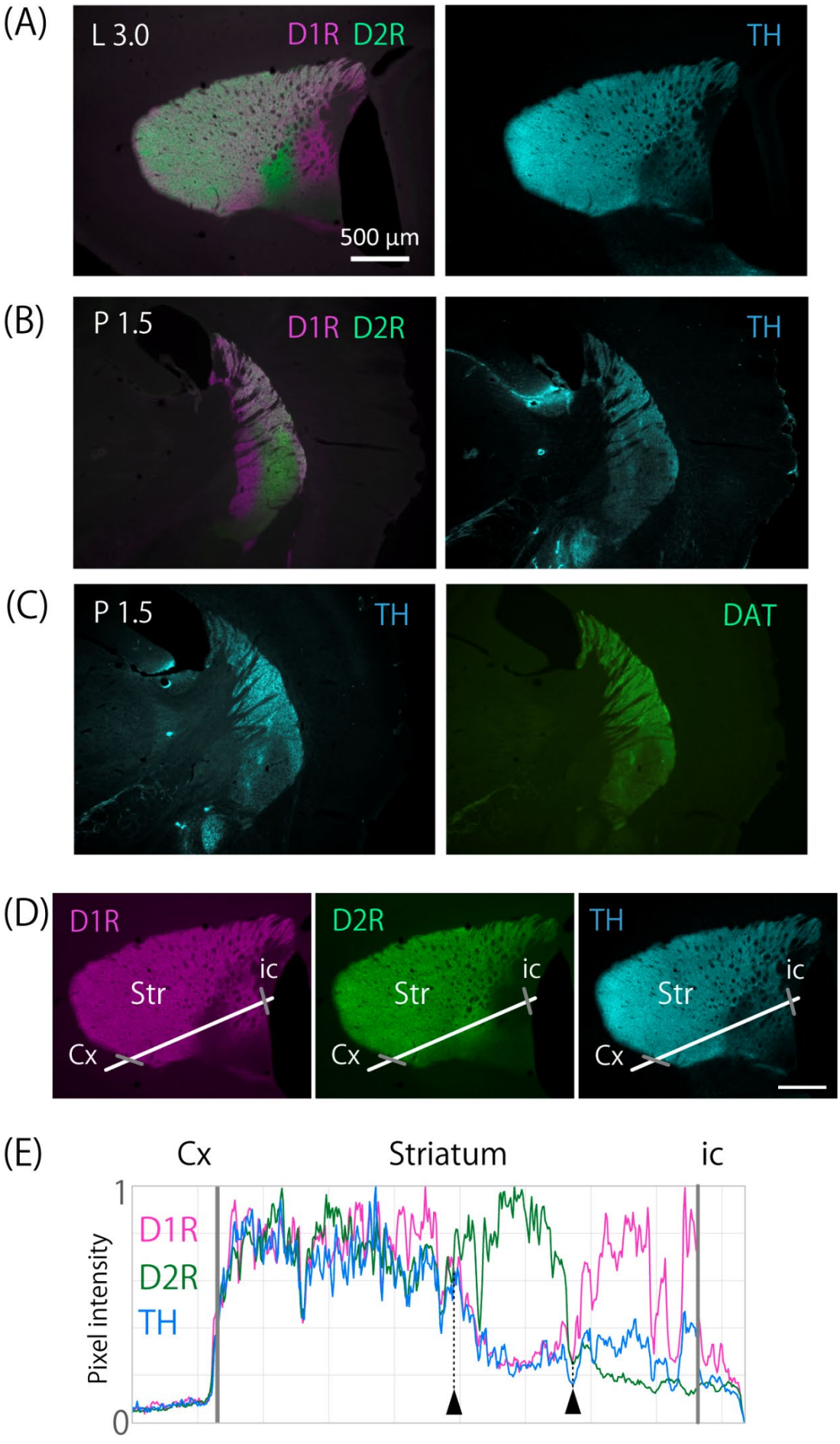
(A)
L 3.0
D1R D2R
500 µm
TH
(B)
P 1.5
D1R D2R
TH
(C)
P 1.5
TH
DAT
(D)
D1R
Str
ic
Cx
D2R
Str
ic
Cx
TH
Str
ic
Cx
(E)
Cx
Striatum
ic
1
0
Pixel intensity
D1R
D2R
TH

Fig. 6 Distribution of immunoreactivities related to dopamine and pixel intensity line plot for D1R, D2R, and TH in the caudal lateral striatum

Triple immunofluorescence labeling for D1R (magenta), D2R (green), and TH (cyan) in a sagittal section (A) and a coronal section (B). (C) Double immunofluorescence labeling for TH (cyan) and dopamine transporter (DAT; green). (D) Triple immunofluorescence labeling for D1R (magenta), D2R (green), and TH (cyan) in a sagittal section. The white lines were drawn rostrocaudally to cross the middle of D1R-poor zone and D2R-poor zone and run parallel to the boundary between the Str and the ASt, and traversed the cortex (Cx), the Str, the D1R- and D2R-poor zones, and the internal capsule (ic). The gray lines indicate the boundary between the Cx and the Str or between the Str and the ic. (E) Pixel intensity line plot of triple fluorescent signals (1 pixel = 14.24 μm^2; no signal = 0, maximum level = 255). The colored lines (D1R: magenta, D2R: green, TH: cyan) indicate the fluctuation of the pixel intensity along with the lines in panel D. The pixel intensity for each color was normalized to the highest value for that color. The gray lines indicate the boundary of the Str from the Cx and the ic. The two black arrowheads show the crossing points of the lines for D1R and D2R.

To further test whether the low immunoreactivity for TH was a reflection of sparse innervation of dopaminergic neurons, we investigated the distribution of dopaminergic axons by injecting AAV-Efla-DIO-EGFP into TH-Cre mice, resulting in GFP being expressed specifically in monoaminergic neurons and axons, including dopaminergic neurons, and their axons. As shown in Fig. 7A, we observed rich immunolabeling of GFP throughout the dorsal striatum, but poor immunolabeling of GFP in the D1R- and D2R-poor zones in the caudal lateral striatum, similar to the TH immunolabeling pattern. These results suggest that the D1R- and D2R-poor zones differ from the other striatal areas in terms of dopaminergic input. Furthermore, we also demonstrated that the immunoreactivity for serotonin was high in the TH-poor zone (Fig. 7B). This result suggests the distinct axonal distribution of dopaminergic and serotonergic neurons in the D1R- and D2R-poor zones.

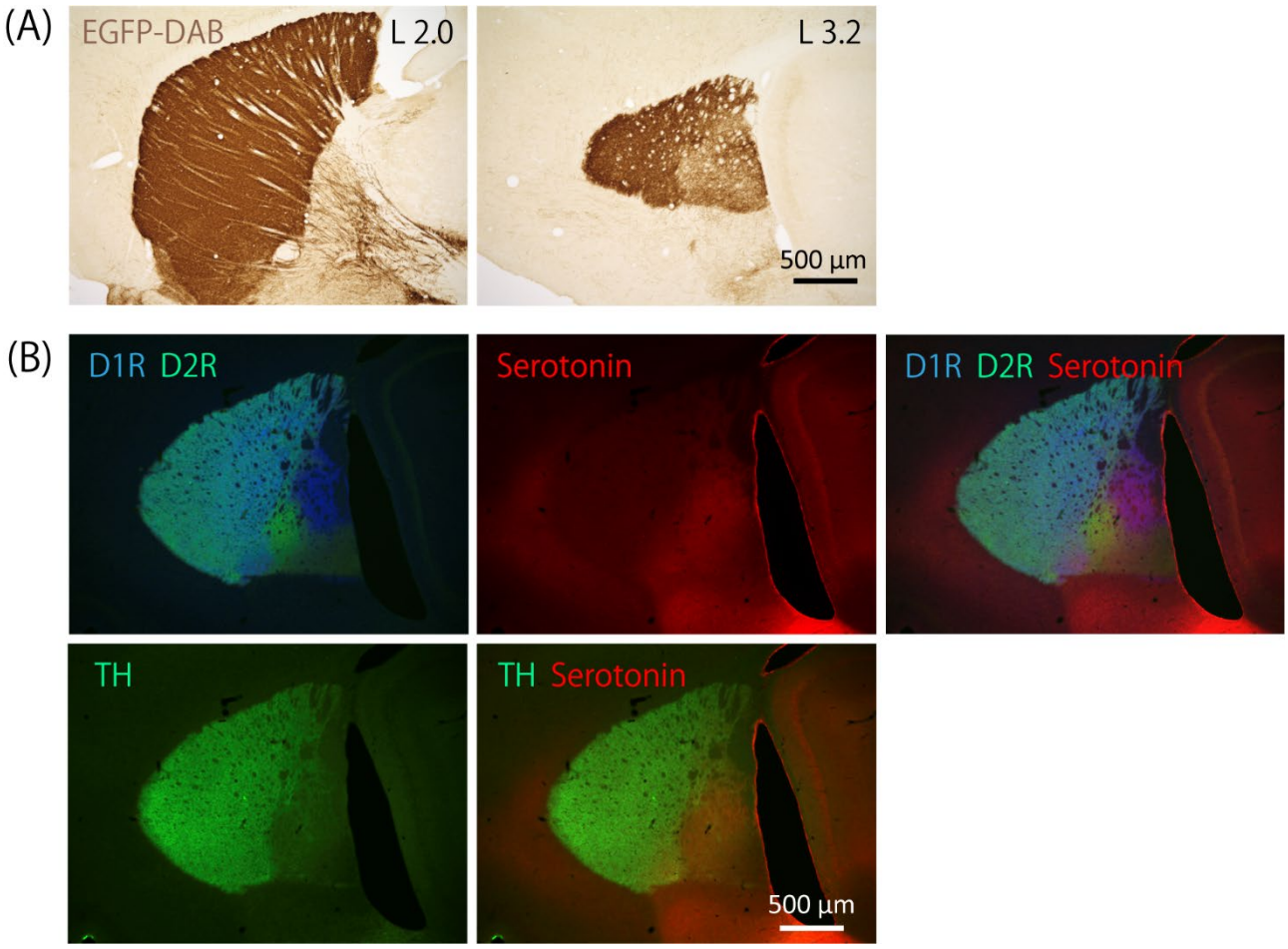

Fig. 7 Efficient labeling of dopaminergic axons using an adeno-associated virus (AAV) vector encoding loxP in TH-Cre mice and distribution of immunoreactivity for serotonin in mice

(A) Diaminobenzidine-4HCl (DAB)-labeled TH-positive dopaminergic axons (brown) in the dorsal medial striatum (L 2.0 mm, left panel) and the caudal lateral striatum (L 3.2 mm, right panel). Note that labeled dopaminergic axons are sparsely distributed in a subregion of the caudal lateral striatum, consistent with the D1R-poor zone. (B) Quadruple immunofluorescence images for D1R (blue), D2R (green; upper row), serotonin (red), and TH (green; bottom row). Note that the immunoreactivity for serotonin was high in the TH-poor zone, consistent with the D1R- and D2R-poor zones.

3. 3. Conservation of the general relationships of D1R-dMSN and D2R-iMSN in the D1R- and D2R-poor zones

It is generally accepted that the direct pathway comprises D1R-expressing MSNs, and that D2R-expressing MSNs correspond to the indirect pathway of the basal ganglia. However, the discovery of the D1R- and D2R-poor zones requires re-evaluation of these relationships. To confirm the density of dMSNs in these distinctive subregions, we injected a retrograde tracer, CTB, conjugated with a fluorophore, into the major output nuclei of the direct pathway—the SNr and the EP (Fig. 8A). We also examined whether retrogradely labeled neurons express D1R mRNA but not D2R mRNA by using in situ hybridization. We found that retrogradely labeled dMSNs were quite widespread in the striatum (Fig. 8B–C), but very few in number in the D1R-poor zone, as expected. Thus, only a few neurons were labeled with the retrograde tracer (Fig. 8C). In contrast, the D2R-poor zone contained a substantially larger number of CTB-positive neurons (Fig. 8C). Cell counting revealed that the density of CTB-positive neurons was significantly lower in the D1R-poor zone, but significantly higher in the D2R-poor zone than that in both the rDS and cDS (**$p < 0.01$; *$p < 0.05$; D1R poor zone vs rDS, $p = 0.0017$; D1R poor zone vs cDS, $p = 0.00067$; D2R poor zone vs rDS, $p = 0.0090$; D2R poor zone vs cDS, $p = 0.030$; D1R poor zone vs D2R poor zone, $p = 3.2\times10^{-5}$; N = 3 sections from three mice). No difference was observed in the density of labeled neurons between the rDS and cDS (rDS vs cDS, $p = 0.79$) (Fig. 8D). These results suggest that the D1R- and D2R-poor zones have different densities of dMSNs as compared to the other striatal areas. However, despite the large difference in the density of dMSNs, all CTB-positive neurons in both the D1R- and D2R-poor zones

expressed D1R mRNA, but not D2R mRNA (Fig. 8E–F). Therefore, these results indicate that the projection pattern, of D1R-expressing MSNs projecting directly to the output nuclei, is well conserved in the D1R- and D2R-poor zones of the caudal lateral striatum.

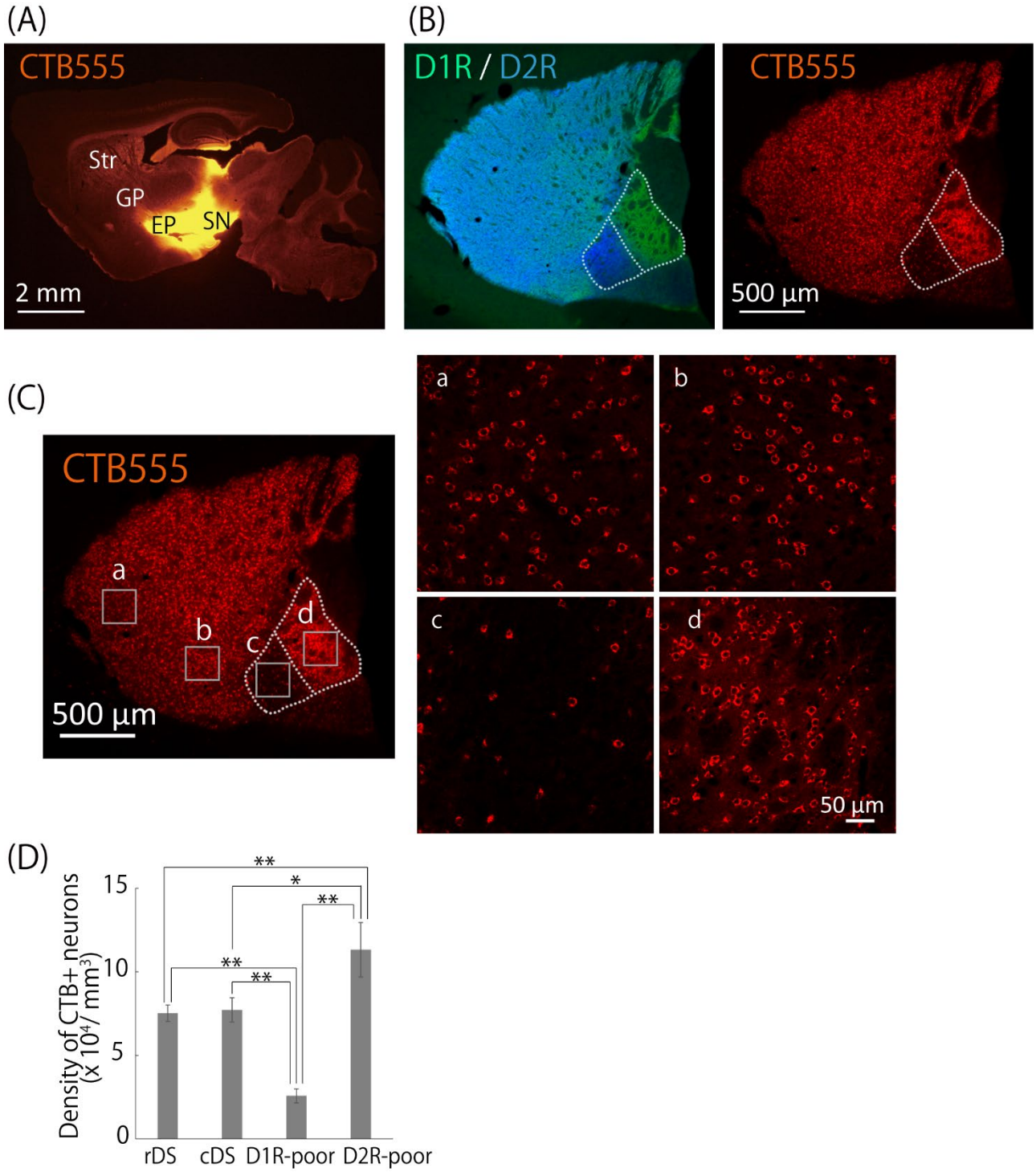

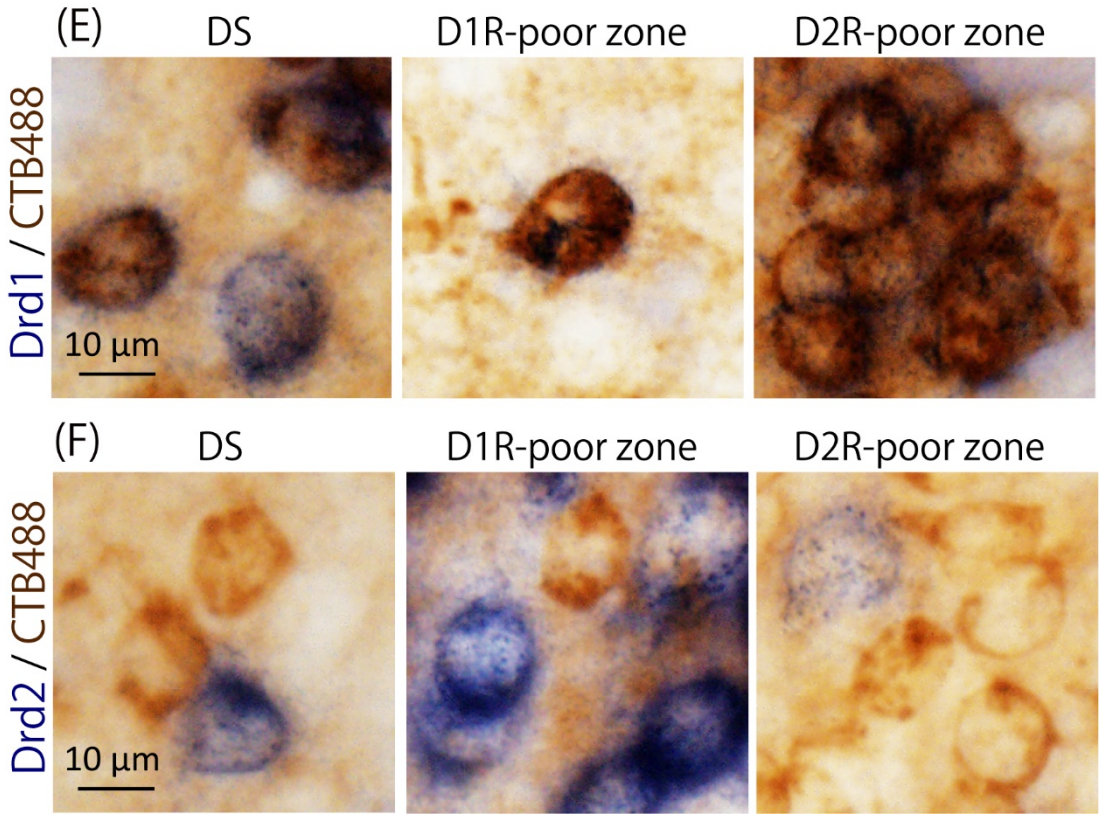

Fig. 8 Retrograde labeling of dMSNs by injecting choleratoxin subunit B – AlexaFluor 555 conjugate (CTB555) into basal ganglia output nuclei in mice

(A) Low-magnification image displaying the injection site, extended to the SNr, the SNc, the STN, and the EP, but not the GP. (B) Overlay of fluorescence images for D1R (green), D2R (blue; left), and neurons retrogradely labeled with CTB555 (red; right) in the caudal lateral striatum. (C) Distribution of retrogradely labeled neurons among the four different areas in the striatum: the rDS (a), cDS (b), D1R-poor zone (c), and D2R-poor zone (d). Note that there are fewer retrogradely labeled neurons in the D1R-poor zone than in the DS, but that the density is higher in the D2R-poor zone than in the DS. (D) CTB555+ neuron density in the four areas. Note that the density was significantly lower in the D1R-poor zone than in the DS, but significantly higher in the D2R-poor zone than in the DS (*$p < 0.05$, **$p < 0.01$, 3 animals, 1 section/animal). (E), (F) dMSNs retrogradely labeled with CTB488 (brown) and D1R mRNA or D2R mRNA (dark blue). The retrogradely labeled neurons were positive for D1R mRNA (E) but negative for D2R mRNA (F) in both the D1R- and D2R-poor zones. Note that, like dMSNs in other striatal area, dMSNs in the D1R- and D2R-poor zones express D1R but not D2R.

It is generally accepted that D1R-positive dMSNs express SP and prodynorphin, while D2R-positive iMSNs express PPE. To confirm whether these protein distribution patterns are conserved in the D1R- and D2R-poor zones, we attempted to examine the immunoreactivity distributions of SP and PPE. We could not determine the distribution pattern of SP and prodynorphin, because we could not find the appropriate antibodies for them. However, we confirmed that the distribution pattern of PPE-positive neurons was consistent with that of neurons expressing D2R mRNA (Fig. 9; N = 3 sections from three mice). Therefore, these results strongly support the notion that the TS contains distinct subregions where dMSNs expressing D1R and iMSNs expressing D2R are separately distributed.

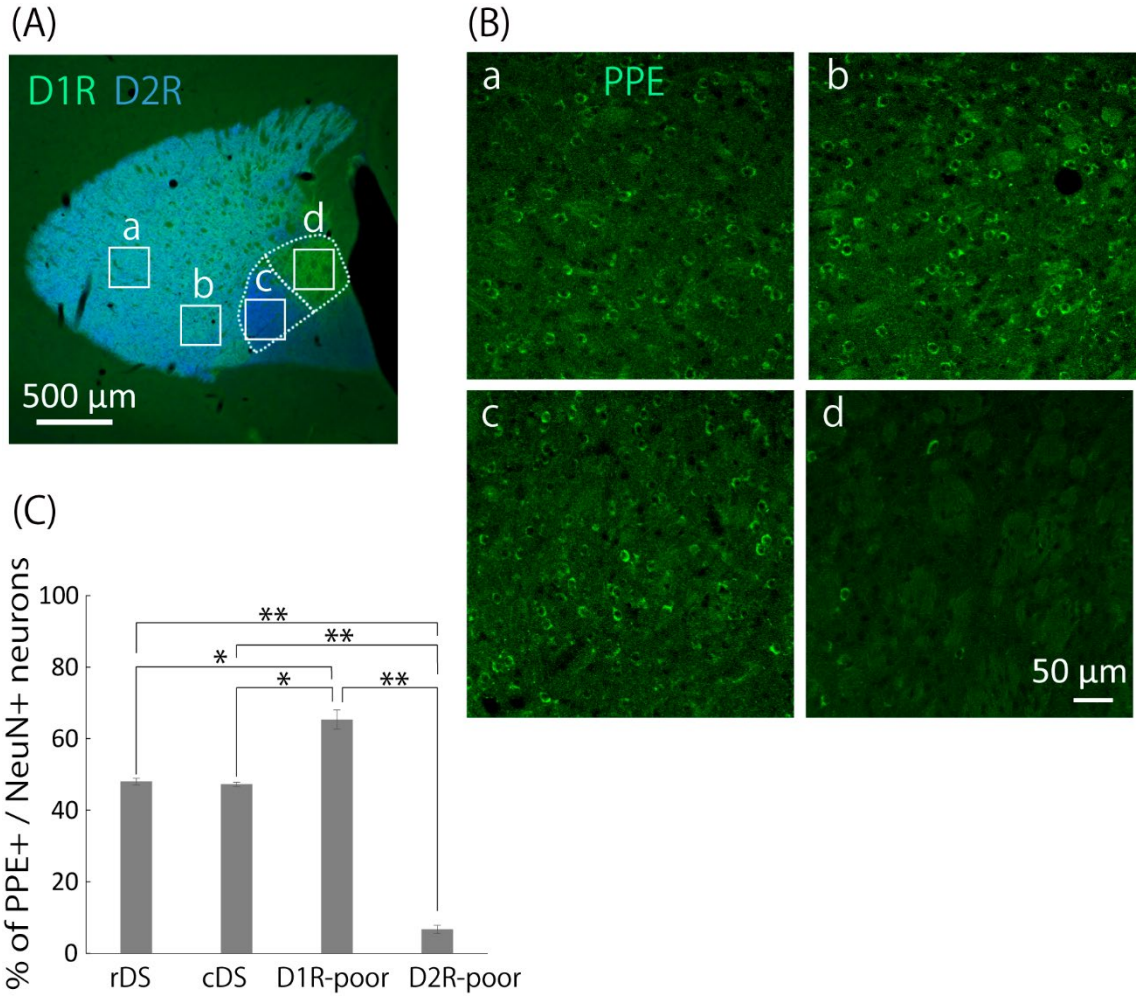

Fig. 9 Distribution of preproenkephalin (PPE)-positive neurons in the caudal lateral striatum
(A) Double immunofluorescence labeling for D1R (green) and D2R (blue). (B) High-magnification immunofluorescence images for PPE in four different areas of A [rDS (a), cDS (b), the D1R-poor zone (c) and the D2R-poor zone (d).] (C) The proportion of PPE+ neurons out of NeuN+ neurons in the four different areas (**$p < 0.01$, *$p < 0.05$, 3 sections, 1 section/animal). Note that the proportion was significantly higher in the D1R-poor zone than in the DS, but significantly lower in the D2R-poor zone than in the DS.

3. 4. Conservation of the D1R- and D2R-poor zones in rodents and primates

We performed all experiments for characterizing the D1R- and D2R poor zones described above on C57BL/6 mice (8–13 weeks old). The caudal lateral striatum is thought to be related to auditory function, because several conventional tracer studies have suggested that it receives inputs preferentially from the auditory cortex (Hannicutt et al., 2016; Hintiryan et al., 2016; Jiang and Kim, 2018). However, C57BL/6 mice are known to develop age-related hearing loss in which hearing in the high-frequency range begins to decline at around 8 weeks and gradually spreads to the low-frequency range (Mikaelian et al., 1974; Suzuki et al., 2016). To confirm that the presence of the D1R- and D2R-poor zones is unaffected by age-related hearing loss, we verified that the zones were present in not only adult C57BL/6 mice but also in young C57BL/6 mice (3 weeks old) (Fig. 10A). Moreover, we investigated whether these distinct striatal subregions are conserved in different strains and species, particularly in primates. We first verified that not only C57BL/6 but also ICR mice showed the D1R- and D2R-poor zones in the caudal lateral striatum, indicating cross-strain conservation (Fig. 10B). Furthermore, similar subregions were observed in Wistar and Long-Evans rats (Fig. 10C–D). In rats, the D1R-poor zone extended from 4.50 mm to 5.50 mm lateral to the midline, and the D2R-poor zone extended from 4.30 mm to 5.30 mm lateral from the midline (Fig. 10C–D). It should be noted that in Long-Evans rats, the shape of the D1R- and D2R-poor zones extended more dorsally than that in mice and Wistar rats (Fig. 10D). In addition to the dopamine receptor heterogeneity, these subregions also had relatively low TH immunoreactivity, as observed in C57BL/6 mice. These results demonstrate that the basic characteristics of the D1R- and D2R-poor

zones are conserved in rodents.

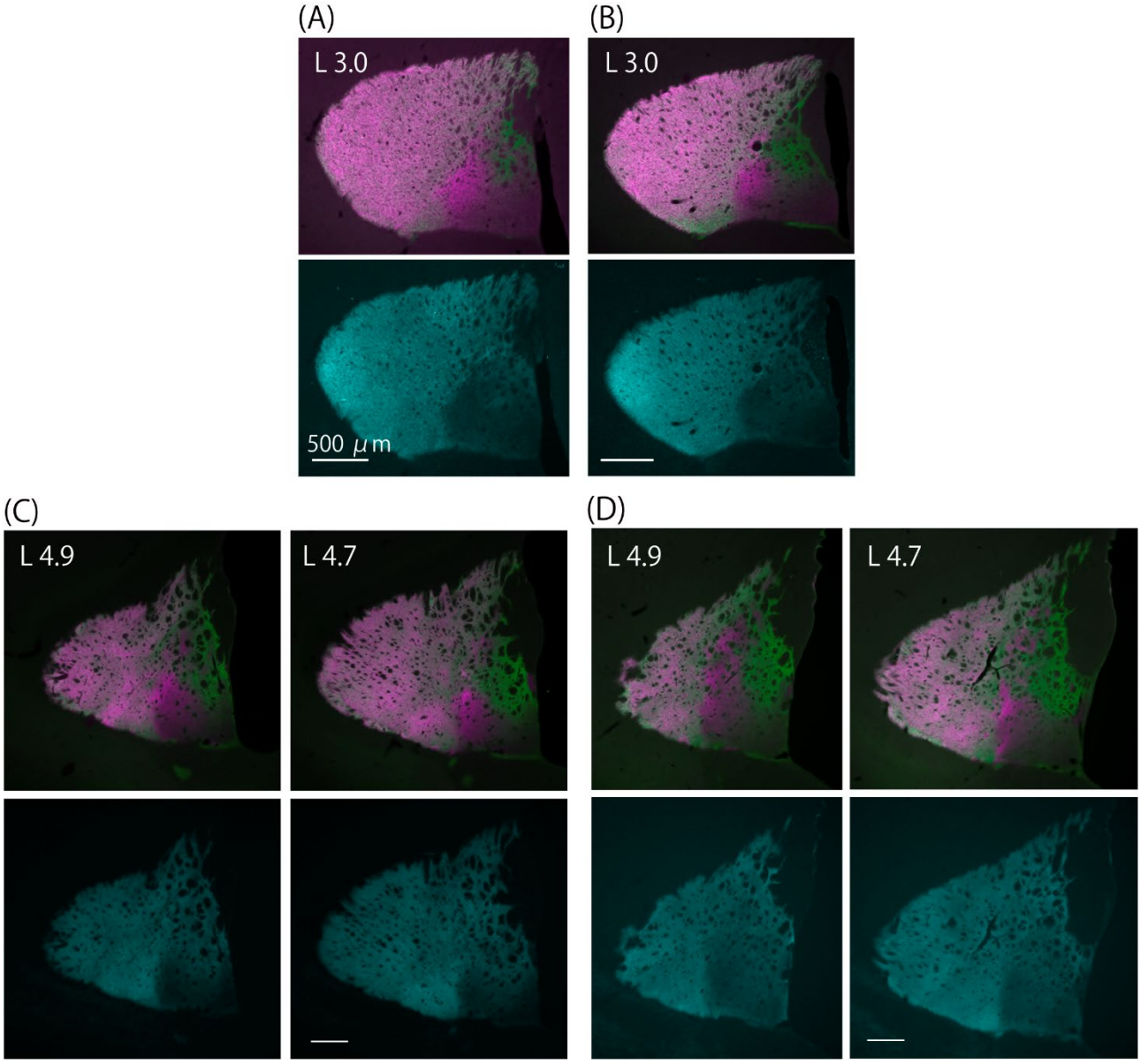

Fig. 10 Distribution of immunoreactivities for D1R, D2R, and TH in mice and rats

Triple immunofluorescence images for D1R (green), D2R (magenta), and TH (cyan) in sagittal sections of the caudal striatum of 3-week young C57BL/6J mouse in sagittal sections [at 3.0 mm lateral from the midline (L 3.0)] (A), ICR mouse in sagittal sections [at 3.0 mm lateral from the midline (L 3.0)] (B), Wistar rat in sagittal sections [from 4.7 mm to 4.9 mm lateral from the midline (L 4.7-4.9)] (C), and Long-Evans rat in sagittal sections [from 4.7 mm to 4.9 mm lateral from the midline (L 4.7-4.9)] (D). Note that the D1R- and D2R-poor zones were found also in young C57BL/6J mice, ICR mice, Wistar rats, and Long-Evans rats. In Long-Evans rats, the shape of the D1R- and D2R-poor zones extended more dorsally than that in mice and Wistar rats.

To investigate whether they are also conserved in primates, we analyzed the striatum of the common marmoset, which is a new-world monkey recently introduced as a primate model for biomedical research. The structure of the striatum in marmosets differs from those of rodents but is similar to that of humans. We first found subregions similar to the D1R- and D2R-poor zones in the CDt of marmosets. The mediolateral positioning of the D1R- and D2R-poor zones was quite similar to that in rodents— “the medial zone / the D2R-poor zone”, “the intermediate zone / the D1R-poor zone”, and “the lateral zone / the other caudate nucleus areas” (Fig. 11A-B). In marmosets, these distinct subregions were located at the edge of the CDt. The D1R-poor zone extended from 7.00 mm to 7.50 mm posterior to the bregma and from 6.30 mm to 7.50 mm lateral from the midline. The D2R-poor zone extended from 7.00 mm to 7.50 mm posterior to the bregma and from 5.70 mm to 6.80 mm lateral from the midline in accordance with the marmoset brain atlas (Paxinos et al., 2011). However, the immunoreactivity for TH was not substantially low in the D1R- and D2R-poor zones of marmosets (Fig. 11A). According to the marmoset gene atlas of the Riken Center for Brain Science, neurons expressing D1R mRNA were substantially sparse in the D1R-poor zone, while very few neurons in the D2R-poor zone expressed D2R mRNA (Fig. 11C). These results show for the first time the presence of unique striatal subregions in the caudal lateral striatum of not only rodents but also primates.

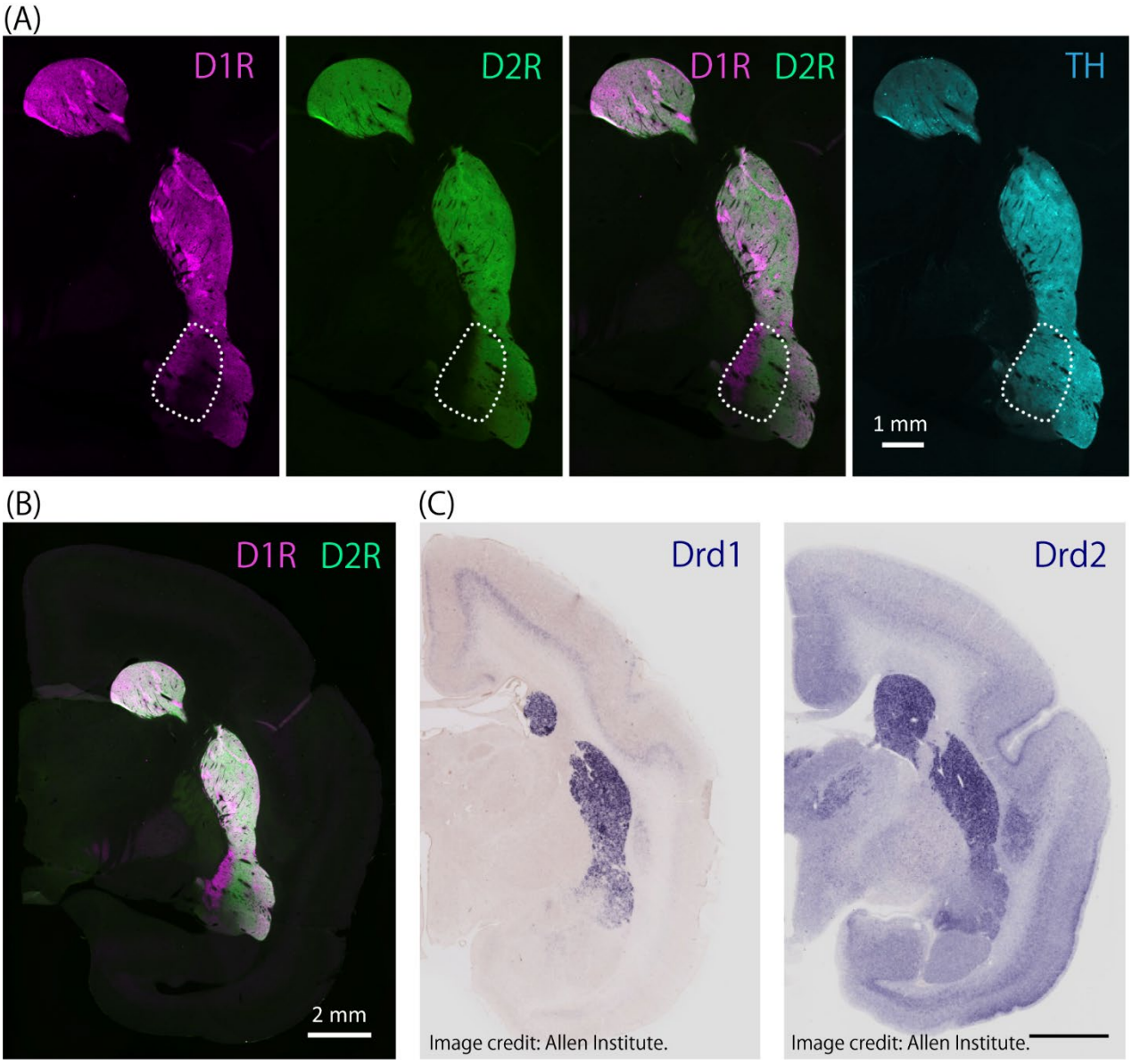

Fig. 11 Distribution of immunoreactivities for D1R, D2R, and TH and mRNA labeling for D1R and D2R in the marmoset tail of the caudate nucleus (CDt)

(A) Triple immunofluorescence images for D1R (magenta), D2R (green), and TH (cyan) in the CDt in a coronal section [at 2.4 mm anterior to the bregma (A 2.4)]. The white dotted lines indicate the contour of the D1R- and D2R-poor zones. Note that the D1R- and D2R-poor zones were also found in the CDt of marmosets; however, the immunoreactivity for TH was not substantially low in the D1R- and D2R-poor zones. (B) Double immunofluorescence image for D1R (magenta) and D2R (green). (C) Labeling for D1R mRNA (left panel) and D2R mRNA (right panel) by in situ hybridization (dark purple) according to the marmoset gene atlas of RIKEN Center for Brain Science. Note that Drd1+ neurons were sparsely distributed in the D1R-poor zone, while Drd2+ neurons were sparsely distributed in the D2R-poor zone.

3. 5. Distinct outputs of striatal neurons in the D1R- and D2R-poor zones

To understand the functions of the D1R- and D2R-poor zones, it is essential to elucidate the corresponding neural circuits. To confirm the output organization of the D1R- and D2R-poor zones, we injected an anterograde tracer, BDA, into the broad range of the D1R-poor zone and the D2R-poor zone (Fig. 12A), the D1R-poor zone (Fig. 12B), and the D2R-poor zone (Fig. 12C). We also injected an anterograde tracer, PHA-L, into the caudal dorsal striatum adjacent to the D1R- and D2R-poor zones (Fig. 12D) to compare their axon distribution. Axons of MSNs in the D1R- and D2R-poor zones were observed in the GP and the SN, especially in the SNL, but not in the EP (Fig. 12A–C). Axons of MSNs in the caudal dorsal striatum were also observed in the GP and the SN, but not in the EP (Fig. 12D).

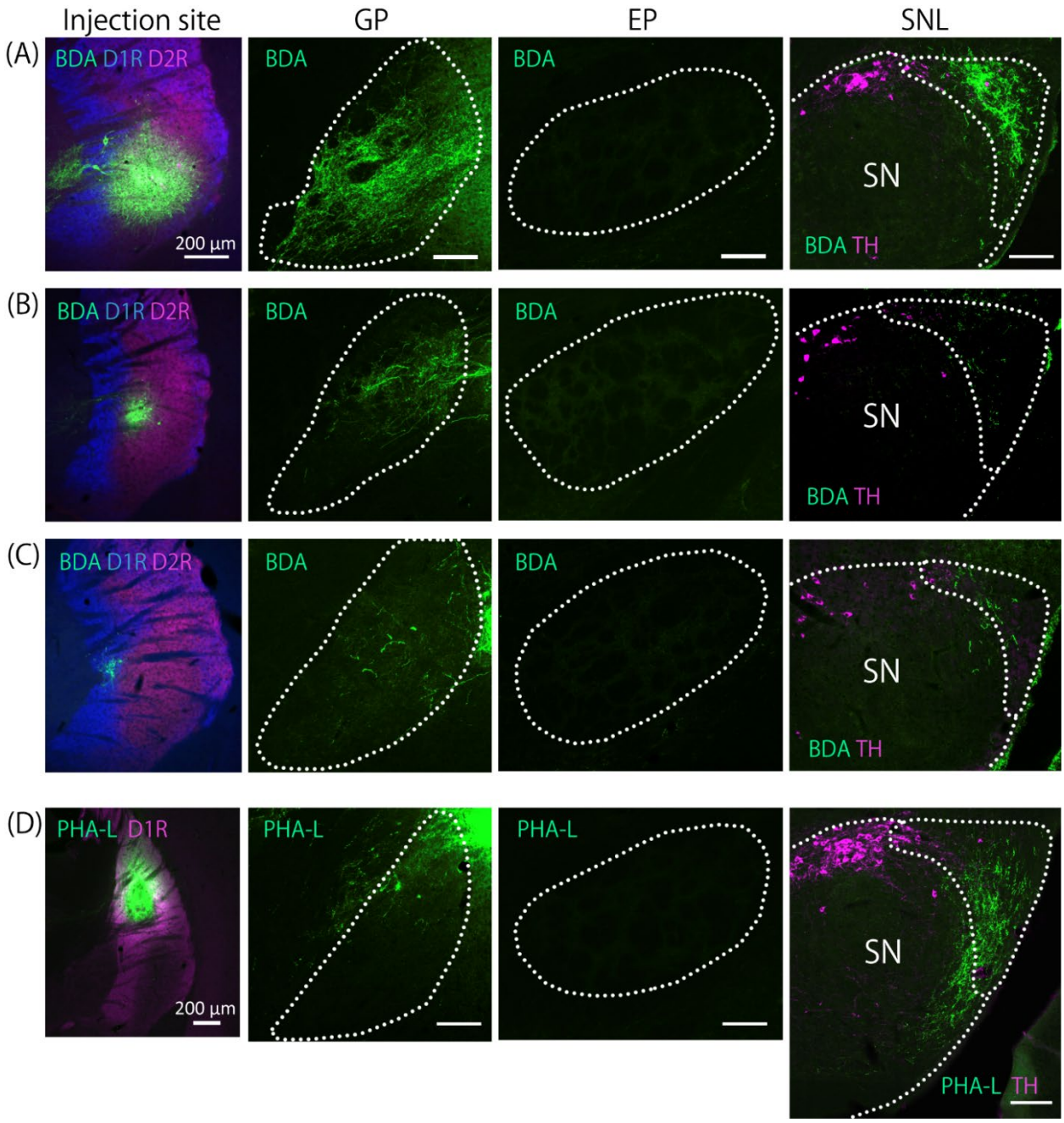

Fig. 12 Axon distribution in the GP, EP, and SN originating from striatal neurons in the D1R-poor zone, the D2R-poor zone, and the caudal dorsal striatum

Fluorescent images on the left show the injection centers for the anterograde tracers [biotinylated dextran amine (BDA; A-C) and *Phaseolus vulgaris* leucoagglutinin (PHA-L; D)] in the D1R- and D2R-poor zones (A), the D1R-poor zone (B), the D2R-poor zone (C), and the caudal dorsal striatum near the D1R-and D2R-poor zones (D). Three fluorescent images on the right show the axon distributions within the GP, EP, and SN, especially in the SNL. The white dotted lines indicate the contours of the GP, EP, and SN. The SNL is the area surrounded by the white dotted line on the right-most fluorescent image. Note that no axon from the caudal lateral striatum, which contains the D1R- and D2R-poor zones and the caudal dorsal striatum, was observed in the EP in all samples we investigated.

According to the Allen Mouse Brain Connectivity Atlas, axons of MSNs in the rostral striatum are distributed in the GP, EP, and SN (Fig. 13A). However, our data indicate that axons of MSNs in the caudal lateral striatum, project to the GP, not to the EP, passed through the ic and the cerebral peduncle, and terminated in the SN (Fig. 13B). One conceivable explanation is the positional relationship of the basal ganglia. The EP is on a line passing through the shortest path from the rostral part of the striatum to the SN. However, the caudal striatum is located lateral to the EP; therefore, in order to take the shortest path from the caudal lateral striatum to the SN, the MSNs in the caudal striatum would not pass through the EP. No significant difference in axon distribution pattern was observed between the D1R-poor zone and the D2R-poor zone (Fig. 12). However, the axon distribution of dMSNs within the SN in the D1R- and D2R-poor zones was substantially different from that in the caudal dorsal striatum. The axons of dMSNs in the D1R-and D2R-poor zones were observed preferentially within the SNL (Fig. 12A-C), while those of dMSNs in the caudal dorsal striatum were observed in the SNL and the lateral part of the SNr lying ventrally along the cerebral peduncle (Fig. 12D).

(A)

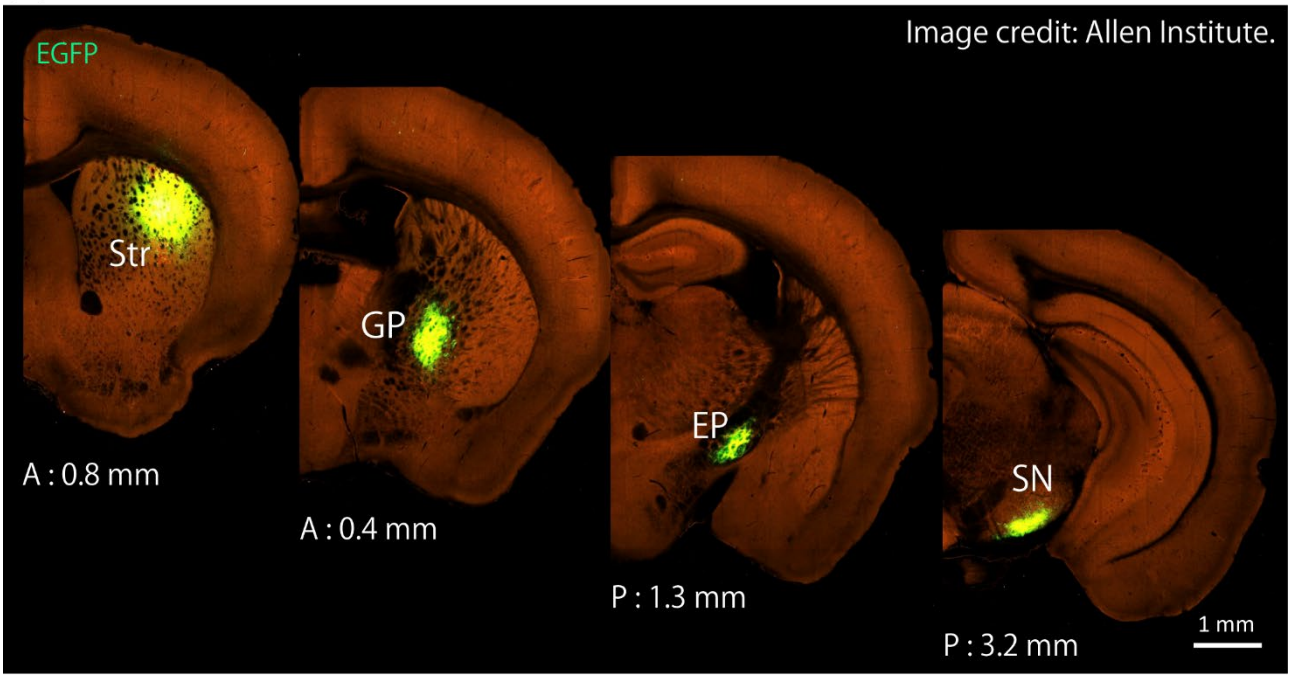
EGFP
Image credit: Allen Institute.
Str
GP
EP
SN
A : 0.8 mm
A : 0.4 mm
P : 1.3 mm
P : 3.2 mm
1 mm

(B)

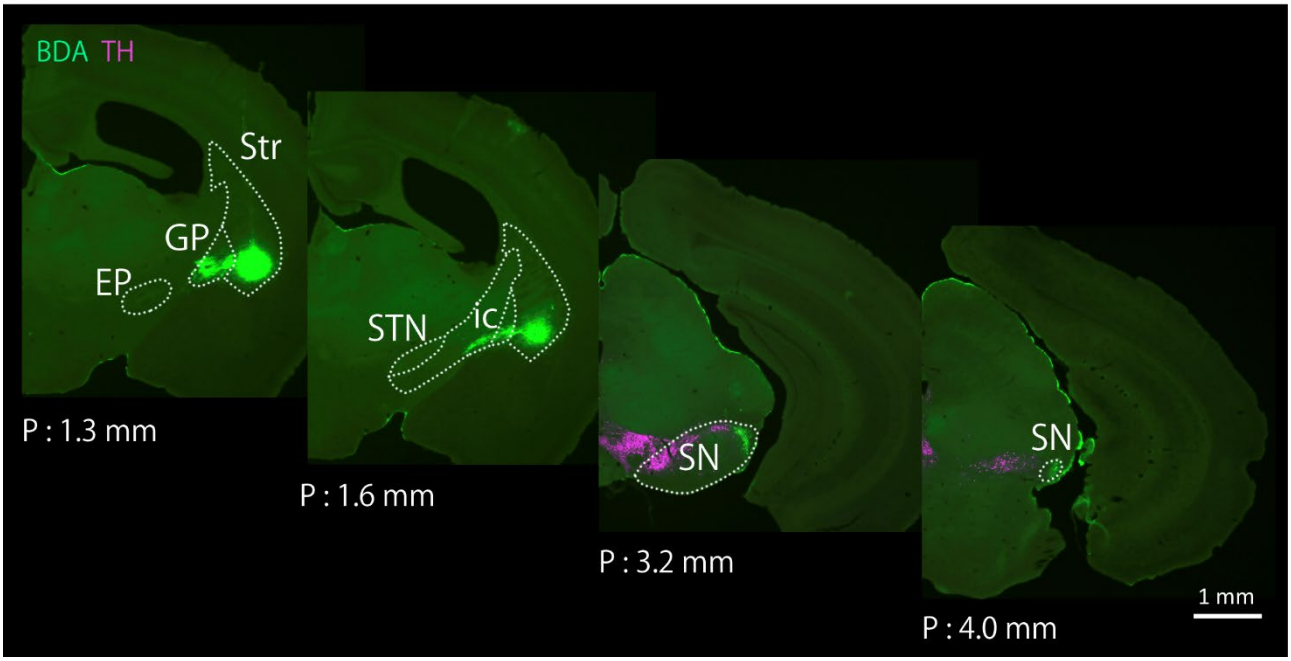
BDA TH
Str
GP
EP
STN
ic
SN
SN
P : 1.3 mm
P : 1.6 mm
P : 3.2 mm
P : 4.0 mm
1 mm

Fig. 13 Distinct pathways of striatal projection neurons in the rostral striatum and the caudal striatum

(A) Fluorescence images for the striatal neuron pathway in the rostral striatum according to the Allen Mouse Brain Connectivity Atlas. The fluorescent image on the left shows the virus injection center in the rostral striatum in a coronal section [at 0.8 mm anterior to the bregma (A: 0.8 mm)]. Axons were observed in the GP, EP, and SN. (B) Fluorescence images for the striatal neuron pathway in the caudal lateral striatum. The fluorescent image on the left shows the injection center for the anterograde tracer, BDA in the caudal striatum and axons in the GP in a coronal section [at 1.3 mm posterior to the bregma (P: 1.3 mm)]. The axons projected to the GP and the SN, passing through the ic. Note that no axon from MSNs in the caudal striatum was observed in the EP in any of our samples.

To quantify their axon distribution, first, we converted the fluorescence images of axon distribution in the SN into binary images and divided the SN into four subregions: the dorsal part of the SNL (dSNL), the ventral part of the SNL (vSNL), the dorsolateral part of the SNr (dlSNr), and the ventrolateral part of the SNr (vlSNr) (Fig. 2, 14E). Next, we measured the proportion of pixels of axons among the four subregions in the SN. The axons of dMSNs in the D1R- and D2R-poor zones most densely distributed in the sections at 3.3 mm posterior to the bregma. No significant differences were observed in the axon distribution pattern among the four subregions in four different injection samples: injection into the D1R- and D2R-poor zones (Fig. 14A), the D1R-poor zone (Fig. 14B), the boundary of the D1R-poor zone and D2R-poor zone (Fig. 14C), and the D2R-poor zone (Fig. 14D). The proportion of the pixels of axons from dMSNs in the D1R- and D2R-poor zones was significantly higher in the dSNL than in the other three subregions, that is the vSNL, dlSNr, and vlSNr (Tukey-Kramer test, **: $p < 0.01$; dSNL vs vSNL, $p = 4.8\times10^{-6}$; dSNL vs dlSNr, $p = 2.7\times10^{-6}$; dSNL vs vlSNr, $p = 4.8\times10^{-7}$; N = 4 sections from three mice) (Fig. 14F). No differences were observed in the proportion of those from dMSNs among the other three subregions (one-way ANOVA; vSNL vs dlSNr, $p = 0.96$; vSNL vs vlSNr, $p = 0.18$; dlSNr vs vlSNr, $p = 0.37$) (Fig. 14F).

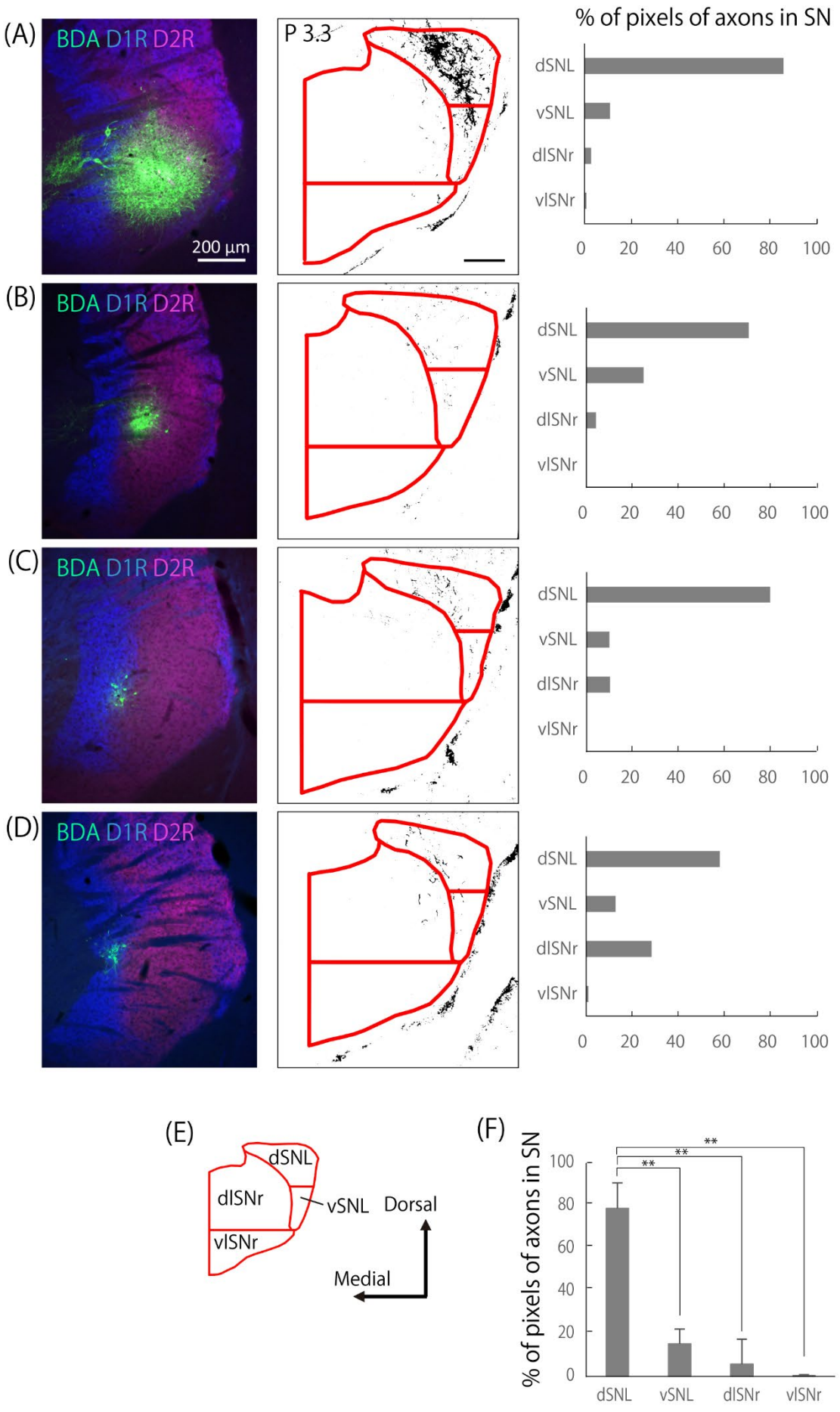
(A)
BDA D1R D2R
200 µm
P 3.3
% of pixels of axons in SN
dSNL
vSNL
dlSNr
vlSNr
0 20 40 60 80 100
(B)
BDA D1R D2R
(C)
BDA D1R D2R
(D)
BDA D1R D2R
(E)
dSNL
dlSNr
vSNL
Dorsal
vlSNr
Medial
(F)
% of pixels of axons in SN
100
80
60
40
20
0
**
**
**
dSNL
vSNL
dlSNr
vlSNr

Fig. 14 Spatial axon distribution of dMSNs in the D1R- and D2R-poor zones among four subregions of the SN

Fluorescent images on the left show the injection centers for the anterograde tracer, BDA, in the caudal lateral striatum subregions: the D1R-and D2R-poor zones (A), the D1R-poor zone (B), the boundary between the D1R-poor zone and D2R-poor zone (C), and the D2R-poor zone (D). The four middle panels show the spatial axon distribution of dMSNs in the D1R-and D2R-poor zones among the four subregions in the SN [the dorsal part of the SNL (dSNL), the ventral part of the SNL (vSNL), the dorsolateral part of the SNr (dlSNr), and the ventrolateral part of the SNr (vlSNr) (E)] for each sample [sections at 3.3 mm posterior to the bregma (P 3.3)]. On the right, the proportion of pixels in axons in each subregion is shown. (F) Proportion of pixels in axons across four samples. One-way ANOVA and Tukey-Kramer test revealed that a significantly larger population of axons was located in the dSNL (**$p < 0.01$, 4 sections, 1 section/animal).

On the other hand, the axons of dMSNs in the caudal dorsal striatum most densely distributed in the sections at 3.5 mm posterior from the bregma, which are more caudal sections than those of the D1R- and D2R-poor zone injection samples (Fig. 15A). The proportion of the pixels of axons from dMSNs in the caudal dorsal striatum, adjacent to the D1R- and D2R-poor zones, did not differ among the four subregions ($p = 0.723$, $N = 3$ sections from three mice; Fig. 15). These results showed that the dMSNs in the D1R- and D2R-poor zones preferentially project to the dSNL, while the dMSNs in the caudal dorsal striatum adjacent to the D1R- and D2R-poor zones project to the SNL and the lateral part of the SNr unbiasedly.

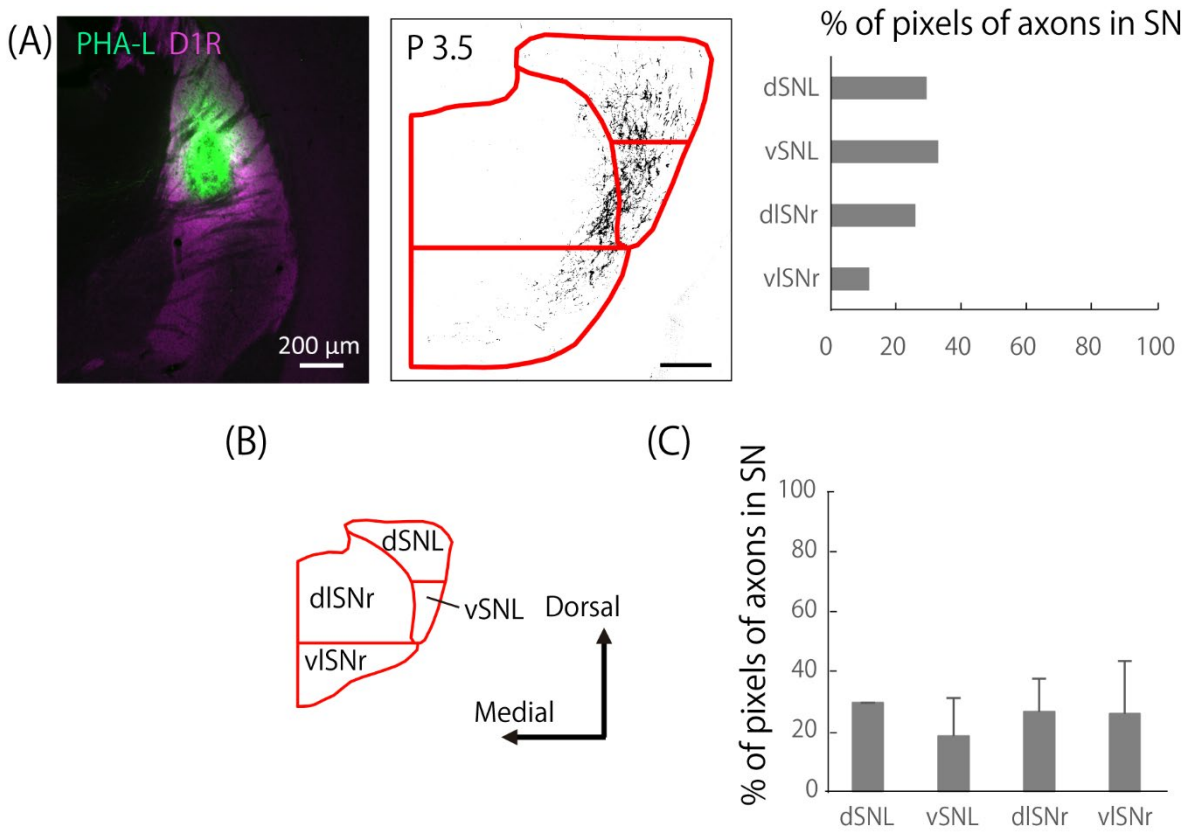

Fig. 15 Spatial axon distribution of dMSNs in the caudal dorsal striatum among four subregions of the SN

(A) Fluorescent image on the left show the injection centers for the anterograde tracer, PHA-L, in the caudal dorsal striatum near the D1R- and D2R-poor zones. The middle panel shows the spatial axon distribution of dMSNs in the caudal dorsal striatum among four subregions in the SN: the dSNL, vSNL, dlSNr, and vlSNr (B) [sections at 3.5 mm posterior to the bregma (P 3.5)]. On the right, the proportion of pixels in axons in each subregion is shown. (C) Proportion of pixels in axons across three samples. One-way ANOVA revealed no significant difference among the four subregions in the SN (3 sections, 1 section/animal).

Furthermore, it is known that the SNL is composed of dopaminergic neurons and PV-positive GABAergic neurons in rodents (Gonzalez-Hernandez and Rodriguez, 2000; Fu et al., 2012). To investigate which types of neurons in the SNL dMSNs in the D1R- and D2R-poor zones project to, we observed axons anterogradely labeled with BDA and immunofluorescence-labelled for TH and PV (Fig. 16A). The labeled axons exhibited close appositions to the soma of PV-positive GABAergic neurons (Fig. 16B (a), (c)), but not to dopaminergic neurons (Fig. 16B (b), (d)) in the SNL. Thus, we also suggest that dMSNs in the D1R- and D2R-poor zones may provide strong inhibition to the PV-positive GABAergic neurons in the SNL, because the soma is where input electrical signals are integrated. A schematic diagram of our new findings on the neural circuits of the D1R- and D2R-poor zones and the caudal dorsal striatum is shown in Fig. 17. The caudal dorsal striatum receives inputs from dopaminergic neurons in the SNc, but less inputs from serotonergic neurons in the dorsal raphe (DR) and medial raphe (MR). Conversely, the D1R- and D2R-poor zones receive inputs from serotonergic neurons in the DR and MR, but less inputs from dopaminergic neurons in the SNc. iMSNs in both the caudal dorsal striatum and the D1R- and D2R-poor zones are thought to project to the GP. dMSNs in the D1R- and D2R-poor zones preferentially project to PV neurons in the SNL, but dMSNs in the caudal dorsal striatum project to the SNr and SNL.

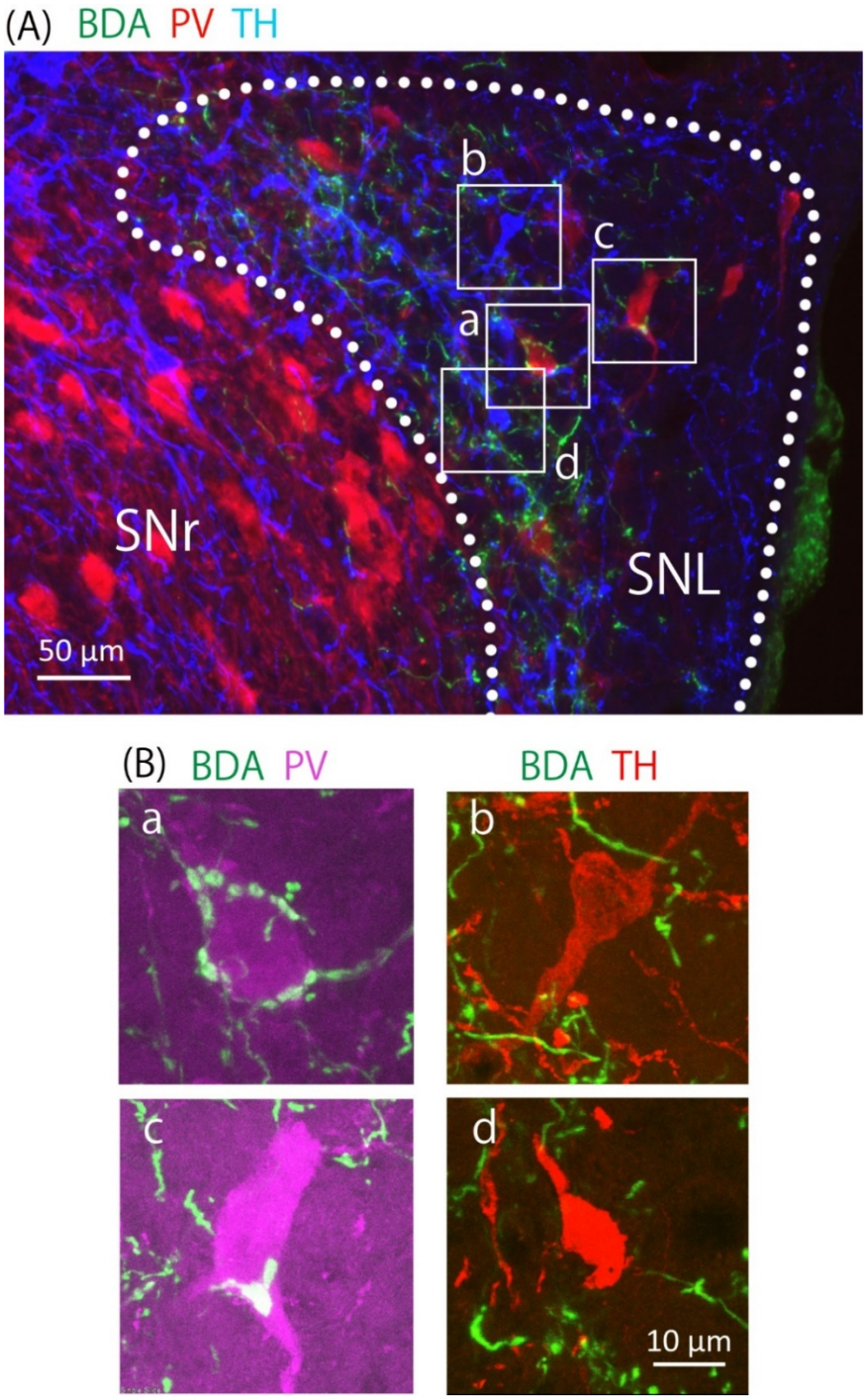

Fig. 16 Axons of dMSNs in the D1R- and D2R-poor zones distributed around the cell body of parvalbumin (PV) neurons in the SNL

(A) Low-magnification fluorescence image for BDA-positive axons (green), PV (red), and TH (blue) in the SNL. White dotted lines indicate the boundary between the SNr and the SNL. (B) High-magnification confocal z-stack fluorescence images of panel A for PV-positive neurons (magenta: a, c), and TH-positive dopaminergic neurons (red: b, d). BDA-positive axons distributed around the cell body (a) or axon initial segment (c) of PV-positive neurons in the SNL. No axon was observed around the cell body of TH-positive dopaminergic neurons in the SNL (b, c).

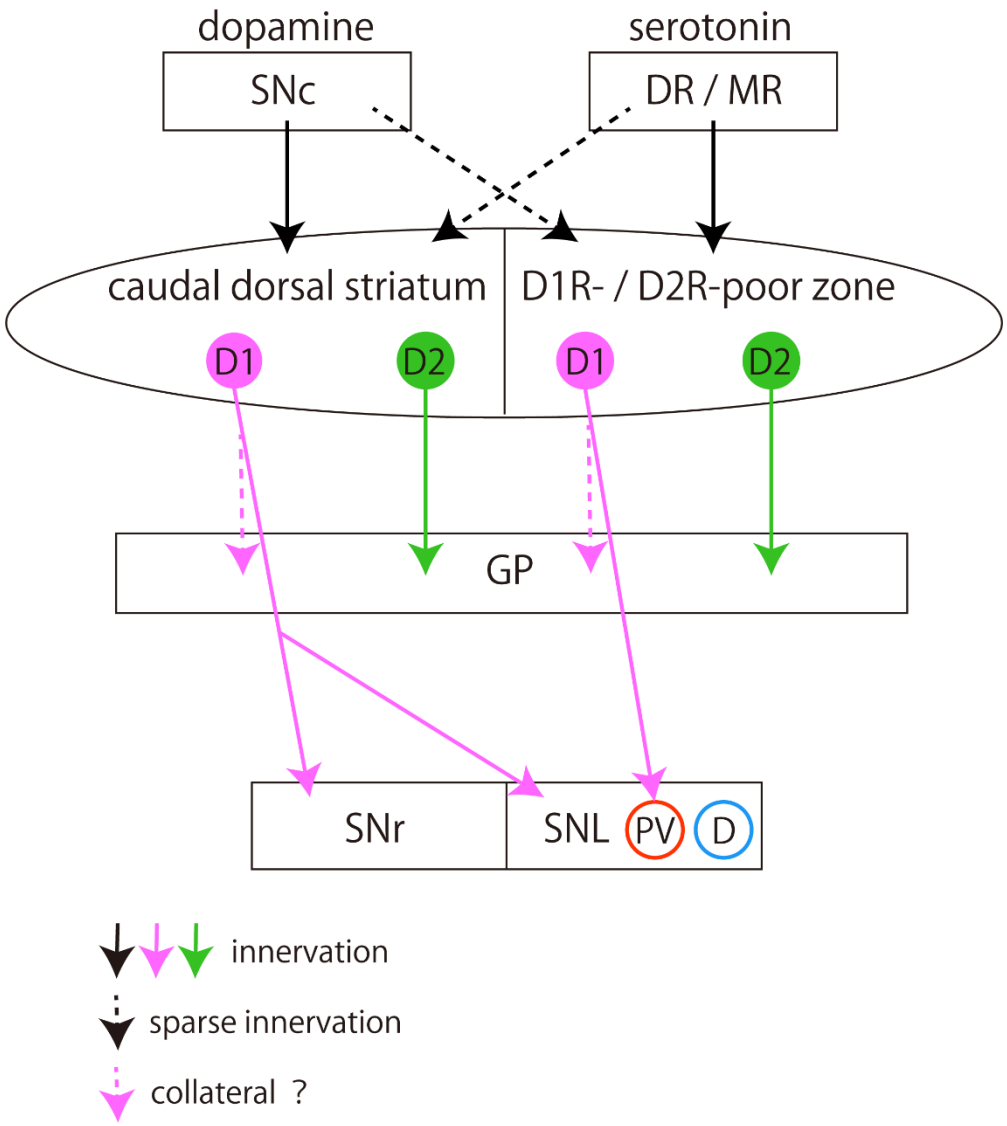

Fig. 17 Schematic diagram of summary

Dopaminergic and serotonergic innervation are shown as black arrows, and their sparse innervation is shown as dashed black arrows. dMSNs innervation is shown as pink arrows. dMSNs in the caudal striatum might have collaterals to the GP (dashed pink arrows), because axons and buttons were observed in the GP of the D2R-poor zone injection sample. iMSNs innervation is shown as green arrows. Red circled PV and blue circled D in the SNL indicate PV neurons and dopaminergic neurons, respectively. The caudal dorsal striatum receives inputs from dopaminergic neurons in the SNc, but less inputs from serotonergic neurons in the dorsal raphe (DR) and medial raphe (MR). Conversely, the D1R- and D2R-poor zones receive inputs from serotonergic neurons in the DR or MR, but less inputs from dopaminergic neurons in the SNc. iMSNs in both the caudal dorsal striatum and the D1R- and D2R-poor zones are thought to project to the GP. dMSNs in the D1R- and D2R-poor zones preferentially project to PV neurons in the SNL, but dMSNs in the caudal dorsal striatum project to the SNr and SNL.

Chapter 4. Discussion

4.1. The D1R- and D2R-poor zones

4.1.1. Molecular expression in the D1R- and D2R-poor zones

In the present study, we showed that the immunoreactivity for D1R was significantly low but that for D2R was intense in the D1R-poor zone, whereas the immunoreactivity for D2R was faint but that for D1R was intense in the D2R-poor zone in rodents and primates (Fig. 3-4). There are at least five subtypes of dopamine receptors: D1, D2, D3, D4, and D5. D1R and D5R are members of the D1-like family of dopamine receptors, whereas D2R, D3R, and D4R are members of the D2-like family (Cools and Rossum, 1975). Although we investigated the distribution of D3R, D4R, and D5R mRNA using the in situ hybridization data from the Allen Brain Atlas, no significant differences were observed among the D1R-poor zone, the D2R-poor zone, and other striatal areas. Borrelli and colleagues reported that D2R exists in two isoforms, a long form (D2L) and a 29 amino-acid shorter form (D2S), both expressed in dopamine neurons as well as in cells receiving dopaminergic afferents (Vallone et al., 2000; Mei et al., 2009). They also reported that D2S preferentially exists in the presynaptic terminals of dopaminergic and glutamatergic neurons, while D2L preferentially exists in postsynaptic neurons like MSNs and interneurons (Mei et al., 2009). The anti-D2R antibodies we used in the experiments in this study detect both D2S and D2L, and there is no anti-D2S antibody. Although we attempted to stain D2L and compare the immunoreactive pattern for D2L with that for D2R, we could not find the appropriate antibodies for D2L. Therefore, we observed the

immunoreactive pattern for D2R detecting both D2S and D2L in dopamine D2L receptor knockout mice (D2L-KO mice), which shows the immunoreactive pattern for D2S. That immunoreactive pattern did not appear to be much different from that for D2R in non-transgenic mice (data not shown). This data suggests that there might be no substantial bias in the distribution of D2S and D2L in the striatum. It is generally accepted that dMSNs express D1R, SP, and prodynorphin, while iMSNs express D2R and PPE (Alexandar and Crutcher, 1990). We elucidated that the intensity of immunoreactivity for D1R and D2R was proportional to the density of dMSNs and iMSNs in the D1R- and D2R-poor zones. A previous study by Miyamoto and colleagues used immunostaining for SP and Enk to determine the boundaries between the D1R-poor zone, the D2R-poor zone, and the other striatal areas. However, despite the large number of D2R-positive neurons in the D1R-poor zone, immunostaining for Enk, which D2R-positive neurons should have, was weak. They explained that the intensity of immunoreactivity for Enk and the iMSNs density were not proportional because Enk was observed in axon terminals, but not in somata. Then, immunoreactive pattern for SP and Enk should not be appropriate to delineate the boundaries between D1R-poor zone, D2R-poor zone, and other striatal areas. Therefore, in order to accurately determine the boundaries of the D1R-poor zone, the D2R-poor zone, and the other striatal areas, immunolabeling for D1R and D2R is necessary instead of immunolabeling for SP and Enk. Nevertheless, our data for the endogenous dopamine receptor proteins showed strong correlations with those obtained for their mRNAs.

4.1.2. Sparse dopaminergic axons and enough dopamine receptors

We demonstrated that immunoreactivity for TH was poor and dopaminergic axons were sparse in both the D1R-poor zone and the D2R-poor zone, indicating sparse innervation of dopaminergic neurons in these distinct subregions. However, the immunoreactivity for D1R was intense in the D2R-poor zone and that for D2R was intense in the D1R-poor zone. Therefore, it can be questioned why D1R- and D2R-poor zones express sufficient D1R and D2R, even though they receive sparse inputs from dopaminergic neurons. One possible hypothesis to answer this question is that D1R and/or D2R could be receptors for something other than dopamine. Of the endogenous ligands, D2R only has an affinity and could be a receptor for dopamine; however, D1R has a high affinity for serotonin, which could work as a partial agonist (Sunahara et al., 1991). In the present study, we showed that the immunoreactivity for serotonin was intense in the D1R-and D2R-poor zones, although no significant difference in the distribution pattern of serotonin receptor mRNA was found based on in situ hybridization according to the Allen Brain Atlas. Therefore, it is possible that serotonin acts as a partial D1R agonist and has an inhibitory effect. Furthermore, based on injecting AAV in the SNc of VgluT2-Cre mice and in situ hybridization, Poulin and colleagues have suggested the possibility that dopaminergic neurons in the SNc co-release dopamine and glutamic acid preferentially to the caudal lateral striatum, which contains the D1R- and D2R-poor zones (Poulin et al., 2018). These observations suggest that the activity control mechanisms in the D1R- and D2R-poor zones differ from those in other striatal areas.

4. 2. Definition of the tail of the striatum in rodents and the tail of the caudate nucleus in primates

4. 2. 1. The location of the tail of the striatum in rodents

The D1R- and D2R-poor zones are thought to be located in the TS, which is reported by Menegas and colleagues (Menegas et al., 2015). They elucidated that dopaminergic neurons projecting to the mouse TS respond to novel cues and reinforce avoidance of threat-related stimuli (Menegas et al., 2017; Menegas et al., 2018). Jian and Kim also used tracers to demonstrate that the rat TS receives inputs from the sensory and value structures (Jian and Kim, 2018). However, the reported location of the TS differs slightly from study to study. In one study (Menegas et al., 2017), the fiber implant location specified as the TS for recording GCaMP signals was as follows: AP, -2.0 mm; LM, 3.25 mm; depth, 2.5 mm. According to our data, that location does not lie within the D1R- and D2R-poor zones, but is located dorsal to these distinct subregions, where the immunoreactivities for both D1R and D2R were high. In a follow-up study (Menegas et al., 2018) too, the location of the optic fiber used to collect GCaMP signals in the TS was located dorsally and rostrally from the D1R- and D2R-poor zones, and did not contain these distinct subregions. In a neural circuit study on rats, the tracer injection site in the TS was also quite dorsal from the D1R- and D2R-poor zones (Jian and Kim, 2018). Thus, the definition and location of the TS remain unclear; however, our present study lays an anatomical foundation to address how to define the TS. To elucidate whether the functions of the D1R- and D2R-poor zones correspond to those noted in the conventional studies mentioned above, further tracer-based studies and behavioral experiments on these distinct subregions are needed.

4. 2. 2. The location of the tail of the caudate nucleus in primates

It remains unclear whether the TS in rodents corresponds to the CDt in primates, because the structure of the striatum in rodents differs from those in primates, as mentioned earlier. However, in the present study, we first elucidated that the D1R- and D2R-poor zones were conserved also in marmosets, an anatomical finding which could be key for elucidating whether there is any homology between the TS in rodents and the CDt in primates. Hikosaka and colleagues have conducted several studies on the distinct functions and neural circuits of the CDh and the CDt in rhesus monkeys (Kim and Hikosaka, 2013; Kim et al., 2014; Kim and Hikosaka, 2015; Griggs et al., 2017). They divided the caudate nucleus into three subregions—the CDh, the caudate body, and the CDt—and then delineated them by the anterior commissure (head-body) and the genu (body-tail). The CDt was along the rostro-caudal axis, and the recording sites and tracer injection sites used by Hikosaka and colleagues were located almost in the middle of the CDt and far away from its edges. However, our study found that the D1R- and D2R-poor zones in marmosets were located at the edge of the CDt. It remains unclear whether the function of the edge of the CDt is similar to that of its middle part. Furthermore, it remains uncertain whether the CDt in marmosets corresponds to the CDt in rhesus monkeys. To answer these questions, it is essential to investigate whether the D1R- and D2R-poor zones are also conserved in the CDt of rhesus monkeys, to ascertain the locations of the distinct subregions, and to re-evaluate the function of the CDt in primates.

4. 3. Preferential inputs from the auditory cortex to the caudal lateral striatum

Recently, many researchers have reported that the caudal lateral striatum of rodents preferentially receives inputs from the auditory cortex and the medial division of the medial geniculate body (MGm), which is the relay nucleus of the auditory pathway (LeDoux et al., 1991; Deniau et al., 1996; Hintiryan et al., 2016; Hunnicutt et al., 2016; Xiong et al., 2015; Jiang and Kim, 2018). In previous studies on the cortico-striatal projectome, the caudal lateral striatum was found to receive inputs from multiple cortical subregions—the auditory, temporal association (TEa), visual, posterior parietal association, orbitofrontal, and somatosensory cortices (Hintiryan et al., 2016; Hunnicutt et al., 2016). Hintiryan and colleagues have reported that primary auditory cortex (AUDp) projections in mice produce a unique dense terminal field in the TS, where projections from most other cortical areas were absent. They also mentioned that dense projections from the TEa filled a gap between the AUDp terminals and the external capsule in this distinct region of the caudal lateral striatum. It should be noted that this location, which they called a unique dense terminal field in the TS, was consistent with the location of the D1R- and D2R-poor zones. This suggests the possibility that the D1R- and D2R-poor zones preferentially receive inputs from the AUDp. According to Tukano and colleagues, the AUDp has a tonotopic map (Storace et al., 2010; Horie et al., 2013; Tsukano et al., 2016; Tsukano et al., 2017a; Tsukano et al., 2017b). Xiong and colleagues demonstrated that the caudal part of the rat auditory cortex, which responds to low-frequency sounds, preferentially projects to the medial part of the caudal lateral striatum, which is supposed to be consistent with the D2R-poor zone. On the other hand, they also reported that the rostral part of the auditory cortex, which responds to high-

frequency sounds, preferentially projects to the lateral part of the caudal lateral striatum, which is supposed to be consistent with the D1R-poor zone (Xiong et al., 2015). These observations suggest that the D1R- and D2R-poor zones receive inputs from specific cortical areas, particularly AUDp, and urge us to investigate whether they may even be organized to have a tonotopic map.

4. 4. Striato-nigral projection from the caudal lateral striatum

In the present study, we elucidated that dMSNs in the D1R- and D2R-poor zones in the caudal lateral striatum preferentially project to the dorsal part of the SNL, while dMSNs in the caudal dorsal striatum project to the SNL and the SNr. Deniau and colleagues have reported that the caudal lateral striatum of rats receives inputs from the auditory related cortex and auditory temporal areas 1, 2 and 3 and projects to the SNL, while the caudal dorsal striatum receives inputs from the visual related cortex, mainly the secondary lateral visual area, and projects to the SNL and the SNr lying ventrally along the cerebral peduncle (Deniau et al., 1996). Our data corresponded to their results, and confirmed the differences in axon distribution between dMSNs in the D1R- and D2R-poor zones and those in the caudal dorsal striatum. The SNL is a particularly prominent structure in primates and corresponds to the hilum of entrance of the striato-pallido-nigral fibers (Francois et al., 1985). Anatomically, the rat SNL is known to have a low density of cell-bodies and to comprise two types of neurons: dopaminergic neurons, which co-express calretinin, calbindin, and cholecystokinin, and PV-positive GABAergic neurons (Gonzalez-Hernandez and Rodriguez, 2000), similar to the mouse SNL (Fu et al., 2012). In the present study, we also suggested that the dMSNs in these distinct

subregions project to the PV-positive neurons in the SNL. A previous tracer-based study by Moriizumi and colleagues showed that GABAergic neurons in the SNL project to the inferior colliculus (IC), which is the auditory-related nucleus (Moriizumi et al., 1992). Considering these results together, we hypothesize that dMSNs in the D1R- and D2R-poor zones receive the inputs preferentially from the AUDp and the MGm and project to the PV-positive neurons in the SNL, which project to the IC, and are supposed to be a part of the auditory pathway (Fig. 18). This hypothesis suggests that the D1R- and D2R-poor zones are involved in functions related to audition. To test this hypothesis, further anatomical studies of neural connections, perhaps using trans-synaptic tracers, would be required in the future.

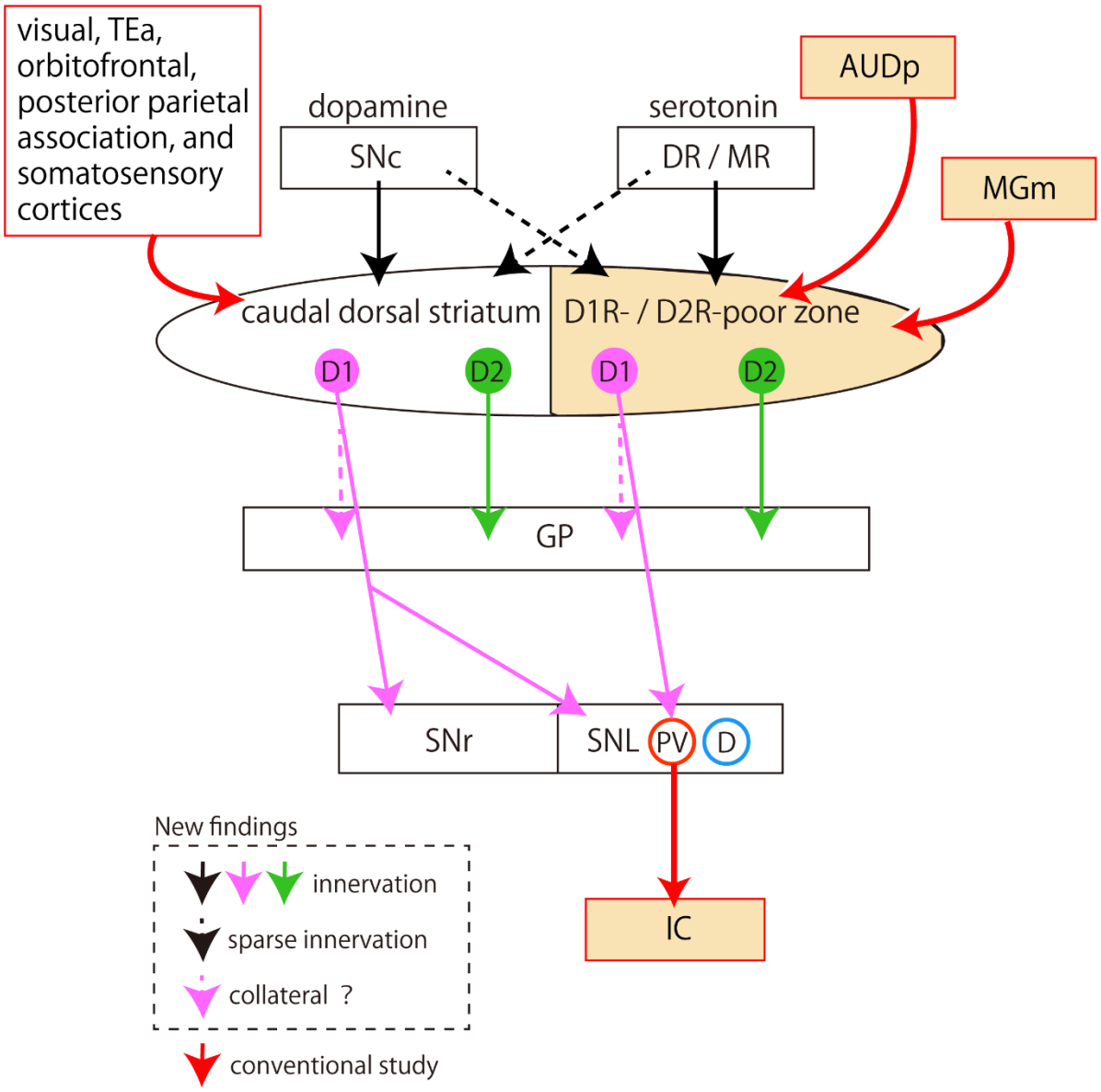

Fig. 18 Schematic diagram of our hypothesis

The neural circuits found in conventional studies are shown as red arrows, and their sparse innervation is shown as dashed black arrows. Dopaminergic and serotonergic innervation are shown as black arrows. dMSNs innervation is shown as pink arrows. dMSNs in the caudal striatum might have collaterals to the GP (dashed pink arrows), because axons and buttons were observed in the GP of the D2R-poor zone injection sample. iMSNs innervation is shown as green arrows. Red circled PV and blue circled D in the SNL indicate PV neurons and dopaminergic neurons, respectively. The caudal dorsal striatum is thought to receive inputs from visual, temporal association (TEa), orbitofrontal, posterior parietal association, and somatosensory cortices. On the other hand, dMSNs in the D1R- and D2R-poor zones are thought to receive inputs preferentially from the primary auditory cortex (AUDp) and the medial division of the medial geniculate body (MGm), and project to PV-positive neurons in the SNL, which project to the inferior colliculus (IC). The D1R- and D2R-poor zones are thought to be a part of the auditory pathway.

Chapter 5. References

Alexander GE, Crutcher MD. Functional architecture of basal ganglia circuits; neural substrates of parallel processing. Trends in neurosciences. 1990:266-271. doi:10.1016/0166-2236(90)90107-l

Bayer HM, Glimcher PW. Midbrain dopamine neurons encode a quantitative reward prediction error signal. Neuron. 2005;47(1):129-141. doi:10.1016/j.neuron.2005.05.020

Bergman H, Feingold A, Nini A, et al. Physiological aspects of information processing in the basal ganglia of normal and parkinsonian primates. Trends in neurosciences. 1997;21(1):1-7.

Bromberg-Martin ES, Matsumoto M, Hikosaka O. Dopamine in Motivational Control: Rewarding, Aversive, and Alerting. Neuron. 2010;68(5):815-834. doi:10.1016/j.neuron.2010.11.022

Clark JJ, Hollon NG, Phillips PEM. Pavlovian valuation systems in learning and decision making. Current Opinion in Neurobiology. 2012;22(6):1054-1061. doi:10.1016/j.conb.2012.06.004

Cohen JY, Haesler S, Vong L, Lowell BB, Uchida N. Neuron-type-specific signals for reward and punishment in the ventral tegmental area. Nature. 2012;482(7383):85-88. doi:10.1038/nature10754

Cools AR, van Rossum JM. Excitation-mediating and inhibition-mediating dopamine-receptors: A new concept towards a better understanding of electrophysiological, biochemical, pharmacological, functional and clinical data. Psychopharmacologia. 1976;45(3):243-254. doi:10.1007/BF00421135

DeLong MR, Crutcher MD, Georgopoulos AP. Primate globus pallidus and subthalamic nucleus: Functional organization. Journal of Neurophysiology. 1985;53(2):530-543.

doi:10.1152/jn.1985.53.2.530

Deniau JM, Menetrey A, Charpier S. The lamellar organization of the rat substantia nigra pars reticulata: Segregated patterns of striatal afferents and relationship to the topography of corticostriatal projections. Neuroscience. 1996;73(3):761-781. doi:10.1016/0306-4522(96)00088-7

Eshel N, Tian J, Bukwich M, Uchida N. Dopamine neurons share common response function for reward prediction error. Nature Neuroscience. 2016;19(3):479-486. doi:10.1038/nn.4239

Chantal Francois, Gerard Percheron, Jerome Yelnik, Simone Heyner. A histological atlas of the macaque (Macaca, mulatta) substantia nigra in ventricular coordinates. Brain Research Bulletin. 1985;14(4):349-367. doi:10.1016/0361-9230(85)90196-0

Fu YH, Yuan Y, Halliday G, Rusznák Z, Watson C, Paxinos G. A cytoarchitectonic and chemoarchitectonic analysis of the dopamine cell groups in the substantia nigra, ventral tegmental area, and retrorubral field in the mouse. Brain Structure and Function. 2012;217(2):591-612. doi:10.1007/s00429-011-0349-2

Gangarossa G, Espallergues J, Mailly P, et al. Spatial distribution of D1R- and D2R-expressing medium-sized spiny neurons differs along the rostro-caudal axis of the mouse dorsal striatum. Frontiers in Neural Circuits. 2013;7(JUL):1-16. doi:10.3389/fncir.2013.00124

Gerfen CR, Surmeier DJ. Modulation of striatal projection systems by dopamine. Annual Review of Neuroscience. 2011;34:441-466. doi:10.1146/annurev-neuro-061010-113641

Gerfen CR. The neostriatal mosaic: striatal patch-matrix organization is related to cortical lamination. Science. 1989;246(4928):385-388. doi:10.1126/science.2799392

García-González D, Khodosevich K, Watanabe Y, Rollenhagen A, Lübke JHR, Monyer H.

Serotonergic Projections Govern Postnatal Neuroblast Migration. Neuron. 2017;94(3):534-549.e9. doi:10.1016/j.neuron.2017.04.013

Griggs WS, Kim HF, Ghazizadeh A, Costello MG, Wall KM, Hikosaka O. Flexible and stable value coding areas in caudate head and tail receive anatomically distinct cortical and subcortical inputs. Frontiers in Neuroanatomy. 2017;11(November):1-19. doi:10.3389/fnana.2017.00106

Hintiryan H, Foster NN, Bowman I, et al. The mouse cortico-striatal projectome. Nature Neuroscience. 2016;19(8):1100-1114. doi:10.1038/nn.4332

Horie M, Tsukano H, Hishida R, Takebayashi H, Shibuki K. Dual compartments of the ventral division of the medial geniculate body projecting to the core region of the auditory cortex in C57BL/6 mice. Neuroscience Research. 2013;76(4):207-212. doi:10.1016/j.neures.2013.05.004

Hunnicutt BJ, Jongbloets BC, Birdsong WT, Gertz KJ, Zhong H, Mao T. A comprehensive excitatory input map of the striatum reveals novel functional organization. eLife. 2016;5(November2016):1-32. doi:10.7554/eLife.19103

Jaeger D, Gilman S, Wayne Aldridge J. Neuronal activity in the striatum and pallidum of primates related to the execution of externally cued reaching movements. Brain Research. 1995;694(1-2):111-127. doi:10.1016/0006-8993(95)00780-T

Jiang H, Kim HF. Anatomical inputs from the sensory and value structures to the tail of the rat striatum. Frontiers in Neuroanatomy. 2018;12(May):1-17. doi:10.3389/fnana.2018.00030

Kim HF, Hikosaka O. Distinct Basal Ganglia Circuits Controlling Behaviors Guided by Flexible and Stable Values. Neuron. 2013;79(5):1001-1010. doi:10.1016/j.neuron.2013.06.044

Kim HF, Hikosaka O. Parallel basal ganglia circuits for voluntary and automatic behaviour to reach

rewards. Brain. 2015;138(7):1776-1800. doi:10.1093/brain/awv134

Kim HF, Ghazizadeh A, Hikosaka O. Separate groups of dopamine neurons innervate caudate head and tail encoding flexible and stable value memories. Frontiers in Neuroanatomy. 2014;8(October):1-12. doi:10.3389/fnana.2014.00120

Kim HF, Ghazizadeh A, Hikosaka O. Dopamine neurons encoding long-term memory of object value for habitual behavior. Cell. 2015; 163(5):1165-1175. doi.org/10.1016/j.cell.2015.10.063.

Kincaid AE, Penney JB, Young AB, Newman SW. Evidence for a projection from the globus pallidus to the entopeduncular nucleus in the rat. Neuroscience Letters. 1991;128(1):121-125. doi:10.1016/0304-3940(91)90774-N

Kita H, Kitai ST. Intracellular study of rat globus pallidus neurons: membrane properties and responses to neostriatal, subthalamic and nigral stimulation. Brain Res. 1991;564:296–305. doi: 10.1016/0006-8993(91)91466-E

Kreitzer AC. Physiology and pharmacology of striatal neurons. Annual Review of Neuroscience. 2009;32:127-147. doi:10.1146/annurev.neuro.051508.135422

Lança AJ, Boyd S, Kolb B, Kooy DVD. The development of a patchy organization of the rat striatum. Developmental Brain Research. 1986;27(1):1-10. doi:10.1016/0165-3806(86)90226-9

LeDoux JE, Farb C, Ruggiero DA. Topographic organization of neurons in the acoustic thalamus that project to the amygdala. Journal of Neuroscience. 1990;10(4):1043-1054. doi:10.1523/jneurosci.10-04-01043.1990

Matsuda W, Furuta T, Nakamura KC, et al. Single nigrostriatal dopaminergic neurons form widely spread and highly dense axonal arborizations in the neostriatum. Journal of Neuroscience.

2009;29(2):444-453. doi:10.1523/JNEUROSCI.4029-08.2009

de Mei C, Ramos M, Iitaka C, Borrelli E. Getting specialized: presynaptic and postsynaptic dopamine D2 receptors. Current Opinion in Pharmacology. 2009;9(1):53-58. doi:10.1016/j.coph.2008.12.002

Menegas W, Bergan JF, Ogawa SK, et al. Dopamine neurons projecting to the posterior striatum form an anatomically distinct subclass. eLife. 2015;4(AUGUST2015):1-30. doi:10.7554/eLife.10032

Menegas W, Babayan BM, Uchida N, Watabe-Uchida M. Opposite initialization to novel cues in dopamine signaling in ventral and posterior striatum in mice. eLife. 2017;6:1-26. doi:10.7554/eLife.21886

Menegas W, Akiti K, Amo R, Uchida N, Watabe-Uchida M. Dopamine neurons projecting to the posterior striatum reinforce avoidance of threatening stimuli. Nature Neuroscience. 2018;21(10):1421-1430. doi:10.1038/s41593-018-0222-1

Mikaelian D.O, Warfield D & Norris Olga. Genetic Progressive Hearing Loss in the C57/M6 Mouse: Relation of Behaviorial Responses to Cochlear Anatomy. Acta Oto-Laryngologica. 1974;77:1(6):327-334. doi:10.3109/00016487409124632

Miyamoto Y, Katayama S, Shigematsu N, Nishi A, Fukuda T. Striosome-based map of the mouse striatum that is conformable to both cortical afferent topography and uneven distributions of dopamine D1 and D2 receptor-expressing cells. Brain Structure and Function. 2018;223(9):4275-4291. doi:10.1007/s00429-018-1749-3

Miyamoto Y, Nagayoshi I, Nishi A, Fukuda T. Three divisions of the mouse caudal striatum differ in the proportions of dopamine D1 and D2 receptor-expressing cells, distribution of dopaminergic axons, and composition of cholinergic and GABAergic interneurons. Brain Structure and Function.

2019;224(8):2703-2716. doi:10.1007/s00429-019-01928-3

Moriizumi T, Hattori T. Separate neuronal populations of the rat globus pallidus projecting to the subthalamic nucleus, auditory cortex and pedunculopontine tegmental area. Neuroscience. 1992;46(3):701-710. doi:10.1016/0306-4522(92)90156-V

Mounir S, Parent A. The expression of neurokinin-1 receptor at striatal and pallidal levels in normal human brain. Neuroscience Research. 2002;44(1):71-81. doi:10.1016/S0168-0102(02)00087-1

Nambu A, Tokuno H, Takada M. Functional significance of the cortico-subthalamo-pallidal "hyperdirect" pathway. Neuroscience Research. 2002;43(2):111-117. doi:10.1016/S0168-0102(02)00027-5

Parent A, Hazrati LN. Functional anatomy of the basal ganglia. I. The cortico-basal ganglia-thalamo-cortical loop. Brain Res. Rev. 1995a;20:91–127. doi:10.1016/0165-0173(94)00007-C

Parent A, Hazrati LN. Functional anatomy of the basal ganglia. II. The place of subthalamic nucleus and external pallidium in basal ganglia circuitry. Brain Research Reviews. 1995b;20(1):128-154. doi:10.1016/0165-0173(94)00008-D

Poulin JF, Caronia G, Hofer C, et al. Mapping projections of molecularly defined dopamine neuron subtypes using intersectional genetic approaches. Nature Neuroscience. 2018;21(9):1260-1271. doi:10.1038/s41593-018-0203-4

Robledo P, Ferger J. Excitatory influence of rat subthalamic nucleus to substantia nigra pars reticulata and the pallidal complex: electrophysiological data. Brain Res. 1990;518:47–54. doi: 10.1016/0006-8993(90)90952-8

Schultz W, Dayan P, Montague PR. A neural substrate of prediction and reward. Science.

1997;275(5306):1593-1599. doi:10.1126/science.275.5306.1593

Schultz W. Predictive reward signal of dopamine neurons. Journal of Neurophysiology. 1998;80(1):1-27. doi:10.1152/jn.1998.80.1.1

Schultz W. Multiple dopamine functions at different time courses. Annual Review of Neuroscience. 2007;30:259-288. doi:10.1146/annurev.neuro.28.061604.135722

Storace DA, Higgins NC, Read HL. Thalamic label patterns suggest primary and ventral auditory fields are distinct core regions. Journal of Comparative Neurology. 2010;518(10):1630-1646. doi:10.1002/cne.22345

Sunahara, R., Guan, HC., O'Dowd, B. et al. Cloning of the gene for a human dopamine D5 receptor with higher affinity for dopamine than D1. Nature. 1991;350:614–619. doi:10.1038/350614a0

Suzuki M, Sakamoto T, Kashio A, Yamasoba T. Age-related morphological changes in the basement membrane in the stria vascularis of C57BL/6 mice. Eur Arch Otorhinolaryngol. 2016;273(1):57-62. doi: 10.1007/s00405-014-3478-4.

Tsukano H, Horie M, Hishida R, Takahashi K, Takebayashi H, Shibuki K. Quantitative map of multiple auditory cortical regions with a stereotaxic fine-scale atlas of the mouse brain. Scientific Reports. 2016;6(February):1-12. doi:10.1038/srep22315

Tsukano H, Horie M, Ohga S, et al. Reconsidering tonotopic maps in the auditory cortex and lemniscal auditory thalamus in mice. Frontiers in Neural Circuits. 2017;11(February):1-8. doi:10.3389/fncir.2017.00014

Tsukano H, Horie M, Takahashi K, Hishida R, Takebayashi H, Shibuki K. Independent tonotopy and thalamocortical projection patterns in two adjacent parts of the classical primary auditory cortex in

mice. Neuroscience Letters. 2017;637:26-30. doi:10.1016/j.neulet.2016.11.062

Vallone D, Picetti R, Borrelli E. Structure and function of dopamine receptors. Neuroscience and Biobehavioral Reviews. 2000;24(1):125-132. doi:10.1016/S0149-7634(99)00063-9

Wichmann T, Bergman H, DeLong MR. The primate subthalamic nucleus. III. Changes in motor behavior and neuronal activity in the internal pallidum induced by subthalamic inactivation in the MPTP model of parkinsonism. Journal of Neurophysiology. 1994;72(2):521-530. doi:10.1152/jn.1994.72.2.521

Xiong Q, Znamenskiy P, Zador AM. Selective corticostriatal plasticity during acquisition of an auditory discrimination task. Nature. 2015;521(7552):348-351. doi:10.1038/nature14225